A General Stance Stability Test Based on Stratified Morse Theory With Application to Quasi-Static Locomotion Planning

E. Rimon, R. Mason, *Member, IEEE*, J. W. Burdick, *Member, IEEE*, and Y. Or

***Abstract*—This paper considers the stability of an object supported by several frictionless contacts in a potential field such as gravity. The bodies supporting the object induce a partition of the object's configuration space into strata corresponding to different contact arrangements. Stance stability becomes a geometric problem of determining whether the object's configuration is a local minimum of its potential energy function on the stratified configuration space. We use *Stratified Morse Theory* to develop a generic stance stability test that has the following characteristics. For a small number of contacts—less than three in 2-D and less than six in 3-D—stance stability depends both on surface normals and surface curvature at the contacts. Moreover, lower curvature at the contacts leads to better stability. For a larger number of contacts, stance stability depends only on surface normals at the contacts. The stance stability test is applied to quasi-static locomotion planning in two dimensions. The region of stable center-of-mass positions associated with a k-contact stance is characterized. Then, a quasi-static locomotion scheme for a three-legged robot over a piecewise linear terrain is described. Finally, friction is shown to provide robustness and enhanced stability for the frictionless locomotion plan. A full maneuver simulation illustrates the locomotion scheme.**

***Index Terms*—Posture stability, quasistatic locomotion, stance stability, stratified Morse theory.**

I. Introduction

MULTILEGGED robots that perform quasi-static locomotion are becoming progressively more sophisticated. For example, developers of legged robots strive to achieve stable locomotion over uneven terrains, such as staircases [10], complex posture changes, such as sitting and standing up [11], [41], and even cargo lifting [28]. Legged robots are also being deployed in quasi-static climbing scenarios [6], [9], where selection of stable postures is critical for task completion. Whole arm manipulation systems[1] are also becoming progressively more sophisticated in their ability to achieve object manipulation [3], [25], [39], [42]. All of these applications require a fundamental understanding of the static stability properties of an object supported by several contacts against gravity. In particular, the influence of various synthesis parameters, such as number of contacts, surface curvature, and location of center-of-mass on stance stability, must be clearly understood. This paper characterizes the static stability of an object supported by several frictionless contacts in a potential field, such as gravity, making explicit the influence of the aforementioned synthesis parameters on stance stability. While the paper focuses on stances supported by frictionless contacts, it also discusses ways by which friction enhances the stability and robustness of such stances.

Stance stability has received considerable attention in the multilegged locomotion literature. Notable examples are early papers on multilegged machines [18], [24], papers on climbing robots [17], [26], [27], and recent papers on humanoids [10], [11], [14]. Stance stability is also considered in the grasping literature. Notable examples are papers on sensorless manipulation [1], [7], and papers on object recognition [13], [22]. However, with the exception of Trinkle *et al.* discussed later, all these papers make specific assumptions on the terrain geometry or limit the number of contacts. This paper characterizes stance stability over general piecewise smooth terrains with no limitation on the number of contacts. Moreover, the stability test may be useful for applications other than quasi-static locomotion. Examples are whole arm manipulation [3], [29], manipulation of assemblies [2], [23], and control of underwater vehicles subjected to weight-and-buoyancy potential field [15].

A key to the stance stability test is a geometric characterization of the object's configuration space (*c-space*). This space is naturally partitioned into lower dimensional manifolds called *strata*, each corresponding to a particular contact arrangement of the object with the supporting bodies. The stance stability test consequently becomes a geometric problem of determining whether the stance's configuration is a local minimum of the object's potential energy in the stratified c-space. This question has a fully general answer under *stratified Morse theory* (SMT). Kriegman was the first to use SMT in the analysis of stable poses under gravity [13]. However, his work is concerned with objects lying on a flat plane, while this paper is concerned with objects supported by general terrains. Blind *et al.* appeal to the

Manuscript received August 6, 2007. This paper was recommended for publication by Associate Editor O. Brock and Editor K. Lynch upon evaluation of the reviewers' comments.

E. Rimon and Y. Or are with the Department of Mechanical Engineering, Technion-Israel Institute of Technology, Haifa 32000, Israel (e-mail: rimon@technion.ac.il; izi@technion.ac.il).

R. Mason is with the Department of Mechanical Engineering, California Institute of Technology (Caltech), Pasadena, CA 91125 USA. He is also with the RAND Corporation, Santa Monica, CA 90401-3208 USA (e-mail: mason@rand.org).

J. W. Burdick is with the Department of Mechanical Engineering, California Institute of Technology (Caltech), Pasadena, CA 91125 USA (e-mail: jwb@robotics.caltech.edu).

Color versions of one or more of the figures in this paper are available online at http://ieeexplore.ieee.org.

Digital Object Identifier 10.1109/TRO.2008.919287

[1] In these systems, an object is manipulated by one or more articulated mechanisms that are allowed to establish multiple mid link contacts with the manipulated object [4].

principles of SMT in the manipulation of a polygonal part in a 2-D gravitational field [5]. This paper provides a self-contained review of SMT, then develops a general stance stability test that applies to 2-D as well as 3-D terrains. Trinkle *et al.* characterized the stability of polyhedral objects supported by a frictionless whole arm against gravity using a linear complementarity approach [39], [40]. Our SMT approach is completely different. It extends their results to nonpolyhedral objects, while providing a closed-form test that is more useful for synthesis applications.

The stance stability test has the following properties. First, for a given k-contact stance, the only free parameter in the stability test is the location of the object's center-of-mass. One can use this feature to characterize the stable center-of-mass positions of a legged mechanism maintaining a fixed set of contacts with the environment. Second, for a small number of contacts—less than three in 2-D and less than six in 3-D—stance stability depends both on the surface normals and surface curvatures of the contacting bodies. Moreover, in such cases, lower curvature at the contacts leads to better stability. For larger numbers of contacts, stance stability depends solely on the surface normals. These findings are somewhat analogous to results on curvature-based form closure obtained by the authors [35], [36]. Recall that a rigid object held by several rigid bodies is in *form closure* when all of its local motions are blocked by the surrounding bodies [4]. When the number of contacts is small—up to three contacts in 2-D and up to six contacts in 3-D—curvature effects play an important role in achieving form closure. For a larger number of contacts, only surface normals affect form closure. In some sense, this paper extends form closure theory to objects grasped in the presence of gravity or other potential fields.

The organization and contributions of the paper are as follows. The next section reviews basic c-space terminology. Section III reviews relevant aspects of SMT, which forms the basis of the stance stability test. Section IV develops the stance stability test, a key result of the paper. Sections V and VI focus on the application of the stability test to quasi-static locomotion in 2-D. Section V characterizes the region of stable center-of-mass locations for the various k-contact stances in 2-D. Section VI describes a quasistatic locomotion scheme for a three-legged robot over a piecewise linear terrain. The locomotion consists of a 3–2–3 gait pattern with bounded contact sliding. Finally, some amount of friction is always present at the contacts. Friction is shown to provide robustness with respect to small foot placement errors, and also yield better stability properties of the frictionless locomotion plan. The concluding section discusses application of the stance stability test to 3-D terrains, as well as the challenge of obtaining a stability test for frictional stances on uneven terrains.

II. C-Space Representation of Equilibrium Stances

Let the object and its supporting bodies be denoted by $\mathcal{B}$ and $\mathcal{A}_1, \ldots, \mathcal{A}_k$. The stability of $\mathcal{B}$ with respect to $\mathcal{A}_1, \ldots, \mathcal{A}_k$ will be analyzed in $\mathcal{B}$'s configuration space, or *c-space*. We review this space and its stratified sets, then characterize equilibrium stances in c-space.

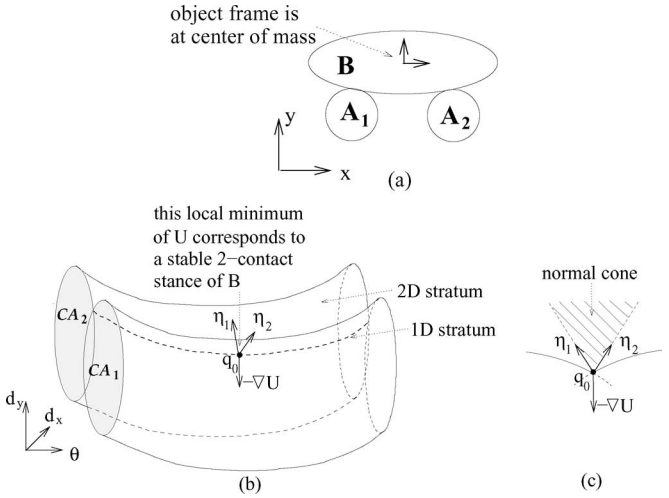

Fig. 1. (a) Object $\mathcal{B}$ supported by two bodies $\mathcal{A}_1$ and $\mathcal{A}_2$. (b) Schematic view of the c-obstacles $\mathcal{CA}_1$ and $\mathcal{CA}_2$ (θ) axis is periodic in 2π). (c) Cross section of the strata at q_0.

A. Configuration Space Review

The configuration space of $\mathcal{B}$ is parametrized by the pair (d, R), where $d \in \mathbb{R}^n$ and $R \in SO(n)$ are the position and orientation of $\mathcal{B}$ relative to a fixed world frame ($n = 2, 3$). In the 3-D case, c-space is parameterized by *hybrid coordinates* $q = (d, \theta)$, where $\theta \in \mathbb{R}^3$ parametrizes $SO(3)$ using exponential coordinates. In the 2-D case, c-space is parameterized by $q = (d, \theta)$, where $\theta \in \mathbb{R}$ parametrizes $SO(2)$. Thus, c-space is parametrized by $\mathbb{R}^m$ where $m = 3$ or 6. From $\mathcal{B}$'s perspective, the supporting bodies form stationary "obstacles." The c-space obstacle (or *c-obstacle*) corresponding to $\mathcal{A}_i$, denoted as $\mathcal{CA}_i$, is the set of $\mathcal{B}$'s configurations at which it intersects $\mathcal{A}_i$. The boundary of $\mathcal{CA}_i$, denoted as $\mathcal{S}_i$, consists of configurations where $\mathcal{B}$ touches $\mathcal{A}_i$ such that the bodies' interiors are disjoint. It can be verified that $\mathcal{S}_i$ is smooth under fairly general conditions. If q_0 is $\mathcal{B}$'s configuration where it is supported by k bodies, q_0 lies on the intersection of $\mathcal{S}_i$ for $i = 1, \ldots, k$. Fig. 1(a) depicts an object supported by two bodies in a planar environment, while Fig. 1(b) schematically shows the c-obstacles corresponding to the two supports.

The free configuration space, or *freespace* $\mathcal{F}$, is the complement of the interior of the c-obstacles in $\mathbb{R}^m$. Starting at a contact configuration q_0, the *free motions* of $\mathcal{B}$ are the curves that emanate from q_0 and locally lie in $\mathcal{F}$. These curves determine the local motions of $\mathcal{B}$ along which it either breaks away from or maintains surface contact with the supporting bodies. The tangent vectors to the free motion curves at q_0 are called the first-order free motions of $\mathcal{B}$ at q_0. In order to characterize the first-order free motions, we need the following notation. Let $\eta_i(q_0)$ be the unit normal to $\mathcal{S}_i$ at q_0, pointing outward with respect to $\mathcal{CA}_i$ (see Fig. 1(b)). The tangent space to $\mathcal{S}_i$ at q_0 is denoted as $T_{q_0}\mathcal{S}_i$, and the tangent space to the ambient c-space is denoted by $T_{q_0}\mathbb{R}^m$. When $\mathcal{B}$ contacts a single body $\mathcal{A}_i$, its first-order free motions are the halfspace: $M(q_0) = \{\dot{q} \in T_{q_0}\mathbb{R}^m : \eta_i(q_0) \cdot \dot{q} \geq 0\}$, pointing away from the c-obstacle at q_0. The boundary of $M(q_0)$ is the

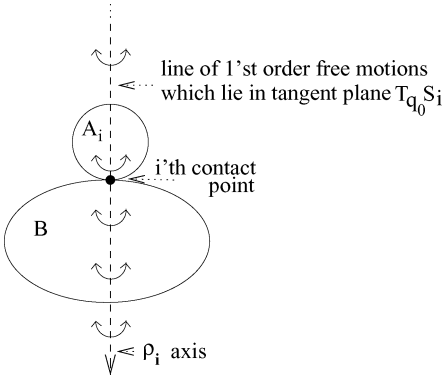

Fig. 2. Parametrization of the tangent first-order free motions of $\mathcal{B}$ with respect to $\mathcal{A}_i$.

tangent space $T_{q_0}\mathcal{S}_i = \{\dot{q} \in T_{q_0}\mathbb{R}^m : \eta_i(q_0) \cdot \dot{q} = 0\}$. When $\mathcal{B}$ contacts k bodies, its first-order free motions are the intersection of its individual free halfspaces:

$$M(q_0) = \{\dot{q} \in T_{q_0}\mathbb{R}^m : \eta_i(q_0) \cdot \dot{q} \geq 0, \text{for } i = 1, \ldots, k\}.$$

Since $M(q_0)$ is the intersection of halfspaces, it is a convex cone that we call the *tangent cone* of $\mathcal{F}$ at q_0.

Remark: The tangent first-order free motions correspond to tangent vectors in $T_{q_0}\mathcal{S}_i$. These first-order free motions can be graphically parametrized, as depicted in Fig. 2. Let l_i denote the line of the ith contact normal. Let ρ_i denote the distance along l_i from the ith contact, such that ρ_i is positive on $\mathcal{B}$'s side of the contact and negative on $\mathcal{A}_i$'s side. Then, the tangent first-order free motions correspond to instantaneous rotations of $\mathcal{B}$ about points on l_i at a distance $\rho_i \in [-\infty, \infty]$. Rotation about an axis at infinity gives pure translation in a direction perpendicular to l_i. Thus, for planar objects, $T_{q_0}\mathcal{S}_i$ can be parametrized by the scalars ρ_i and ω, where ω is the angular velocity about an axis located at a distance ρ_i along l_i.

B. Stratified Sets

The freespace $\mathcal{F}$ is typically a stratified set. A *regularly stratified* set $\mathcal{X}$ is a set $\mathcal{X} \subset \mathbb{R}^m$ decomposed into a finite union of disjoint smooth manifolds[2] called *strata*, satisfying the Whitney condition [8]. The dimensions of the strata vary between zero (isolated point manifolds) and m (open subsets of the ambient space $\mathbb{R}^m$). The Whitney condition requires that the tangents of two neighboring strata "meet nicely," and for our purposes, it suffices to say that this condition is almost always satisfied. The boundary of $\mathcal{F}$ consists of portions of the c-obstacle boundaries. When $\mathcal{B}$ is planar, $\mathcal{F}$ consists of the following strata. The 3-D strata are open subsets of the ambient c-space. The 2-D strata are the portions of the c-obstacle boundaries corresponding to single-body contacts with $\mathcal{B}$. The 1-D strata occur at the intersection of pairs of 2-D strata, and they correspond to two-body contacts with $\mathcal{B}$. The zero-dimensional strata are isolated points that correspond to three-body contacts with $\mathcal{B}$. Fig. 1(b) illustrates the strata formed by two supporting bodies.

[2]Recall that a manifold $\mathcal{M} \subset \mathbb{R}^m$ of dimension d is a hypersurface that locally looks like $\mathbb{R}^d$, for a fixed d in the range $0 \leq d \leq m$.

In order to properly characterize equilibrium stances, we need the notion of critical points on a stratified set. First recall the classical definition of a critical point. Let $\tilde{f}$ be a smooth real-valued function on $\mathbb{R}^m$, and let $\mathcal{M} \subset \mathbb{R}^m$ be a smooth manifold. Let $f : \mathcal{M} \to \mathbb{R}$ denote the restriction of $\tilde{f}$ to $\mathcal{M}$. A point $x \in \mathcal{M}$ is a *critical point* of f if its derivative at x, $Df(x)$, vanishes there. We may characterize the critical points as points $x \in \mathcal{M}$ where the gradient vector $\nabla\tilde{f}(x)$ is normal to the manifold $\mathcal{M}$. A *critical value* of f is the image $c = f(x) \in \mathbb{R}$ of a critical point x. Consider now a stratified set $\mathcal{X} \subset \mathbb{R}^m$, with f denoting the restriction of $\tilde{f}$ to $\mathcal{X}$. The critical points of f are the *union* of the critical points obtained by restricting f to the individual strata of $\mathcal{X}$. In particular, every zero-dimensional manifold is automatically a critical point of f.

C. Representation of Equilibrium Stances

Let $U(q)$ denote a potential energy, such as the gravitational potential, which is defined on the stratified set $\mathcal{F}$ and influences $\mathcal{B}$. Our goal is to characterize the equilibrium points of $\mathcal{B}$ as critical points of U in $\mathcal{F}$. Suppose that $\mathcal{B}$ is at a configuration q_0, supported in static equilibrium by k bodies. At the equilibrium, the net wrench (i.e., force and torque) on $\mathcal{B}$ must be 0. The wrenches acting on $\mathcal{B}$ arise from the potential energy U and from the contact reaction forces. The potential energy wrench is $-\nabla U(q_0)$.[3] The contact reaction wrenches can be described as follows. The wrench due to a normal force applied by $\mathcal{A}_i$ on $\mathcal{B}$ is a positive multiple of the c-obstacle normal $\eta_i(q_0)$ [33]. The collection of all possible reaction wrenches is the set $N(q_0) = \{\sum_{i=1}^{k} \lambda_i \eta_i(q_0) : \lambda_i \geq 0 \text{ for } i = 1, \ldots, k\}$, which we call the *normal cone* of $\mathcal{F}$ at q_0. Thus, a necessary condition for an equilibrium is that there exist nonnegative scalars $\lambda_1, \ldots, \lambda_k$ such that

$$\lambda_1 \eta_1(q_0) + \cdots + \lambda_k \eta_k(q_0) - \nabla U(q_0) = \vec{0}. \tag{1}$$

Equivalently, at an equilibrium configuration, $\nabla U(q_0)$ must lie in $N(q_0)$ (see (Fig. 1(c)). Note that any configuration that satisfies (1) is automatically a critical point of U in $\mathcal{F}$. However, the λ_i's in (1) are required to be nonnegative, while at a general critical point they may attain any sign. (The other critical points correspond to equilibria where $\mathcal{B}$ applies normal suction forces at the contacts. Such suction forces are not considered here.) For frictionless contacts, (1) is not only necessary but also sufficient for an equilibrium stance [21], [32].

III. Review of Relevant Stratified Morse Theory

As discussed in Section IV, the stable equilibria of $\mathcal{B}$ are local minima of the potential energy U on the stratified set $\mathcal{F}$. However, the usual second-derivative test for a local minimum characterizes the local minima only with respect to contact preserving motions. We need SMT to derive the complete stability test that also accounts for contact breaking motions. First we review SMT, then give the condition for a local minimum

[3]Formally, $DU(q)$ is a wrench acting on $\mathcal{B}$, and hence, a covector. Following standard usage, $\nabla U(q)$ is the representation of $DU(q)$ as a tangent vector.

according to this theory. Section IV expresses the local minimum condition in terms of the geometry of the contacting bodies.

As before, $\tilde{f}$ is a smooth real-valued function on $\mathbb{R}^m$, and $f : \mathcal{M} \rightarrow \mathbb{R}$ is the restriction of $\tilde{f}$ to a manifold $\mathcal{M} \subset \mathbb{R}^m$. Then, f is a *Morse function* if all its critical points in $\mathcal{M}$ are nondegenerate, i.e., if its second derivative matrix $D^2 f(x)$ is nonsingular at the critical points. The *Morse index* of f at a critical point x, denoted by σ, is the number of negative eigenvalues of the matrix $D^2 f(x)$. Note that, at a local minimum, all the eigenvalues are positive; hence, $\sigma = 0$. Next consider a regularly stratified set $\mathcal{X} \subset \mathbb{R}^m$, with $f : \mathcal{X} \rightarrow \mathbb{R}$ being the restriction of $\tilde{f}$ to $\mathcal{X}$. Then, f is a *Morse function* on $\mathcal{X}$, if first it is Morse in the classical sense on the stratum containing the critical point x, and second, if $\nabla \tilde{f}(x)$ is *not* normal to any of the other strata meeting at x. The Morse index σ of f at a critical point x is now the number of negative eigenvalues of $D^2 f(x)$ evaluated only on the stratum containing the point x. Thus, $\sigma = 0$ signifies that f has a local minimum on the stratum containing x, but not necessarily with respect to the neighboring strata. By definition, every zero-dimensional stratum is a critical point with Morse index $\sigma = 0$.

SMT is concerned with Morse functions on stratified sets [8]. The theory guarantees that, as the value of f varies between two adjacent critical values of f, the level sets $\mathcal{X}|_c = \{x \in \mathcal{X} : f(x) = c\}$ are *topologically equivalent* (homeomorphic) to each other. Topological changes in the level sets $\mathcal{X}|_c$ must occur locally at the critical points of f. Let x_0 be such a critical point, with $c_0 = f(x_0)$. SMT characterizes the topological change at x_0 in terms of the behavior of f on two complementary subsets of $\mathcal{X}$. The first set is the stratum of $\mathcal{X}$ that contains the critical point x_0, denoted by $\mathcal{S}$. The other set, called the *normal slice* at x_0, is constructed by the following two-stage process. Let $D(x_0)$ be a small disc centered at x_0 and having two properties: the disc intersects the stratum $\mathcal{S}$ only at x_0, and it is transversal to $\mathcal{S}$. The latter requirement is satisfied if one chooses $D(x_0)$ to be normal to $\mathcal{S}$ at x_0, such that $\mathsf{dim}(D(x_0)) = m - \mathsf{dim}(\mathcal{S})$, where $\mathsf{dim}(\cdot)$ denotes dimension. In the second stage, one constructs the normal slice, denoted by $E(x_0)$, as the intersection of $D(x_0)$ with the stratified set $\mathcal{X}$: $E(x_0) = D(x_0) \cap \mathcal{X}$.

The behavior of f on $\mathcal{S}$ is characterized by its Morse index σ at x_0. The behavior of f on the normal slice $E(x_0)$ is determined by its *lower half link* set, denoted by l^-. It is defined as the intersection of $E(x_0)$ with the level set $f^{-1}(c_0 - \epsilon)$: $l^- = E(x_0) \bigcap f^{-1}(c_0 - \epsilon)$, where $\epsilon > 0$ is a small parameter. The topological nature of l^- does not change for all $\epsilon > 0$ sufficiently small [8]. Fig. 3 shows the lower half links of a stratified set $\mathcal{X} \subset \mathbb{R}^3$, which resembles the free space of a planar object. In the figure, $\mathcal{X}$ is formed by removing from $\mathbb{R}^3$ the interior of two smoothly bounded sets $\mathcal{X}_1$ and $\mathcal{X}_2$. The function used in this example is $f(x_1, x_2, x_3) = x_3$, and it has two critical points at x_0 and y_0. The stratum containing these points is a 1-D curve. The normal slice at these points is the intersection with the freespace of a 2-D disc normal to the stratum. At the point x_0, $E(x_0)$ contains no points below x_0, and l^- is empty at x_0. At the point y_0, $E(y_0)$ looks like a downward pointing 2-D sector. The lower half link at y_0, being the intersection of this sector with a horizontal plane lying just below y_0 [the level set $f^{-1}(c_0 - \epsilon)$], is a line segment. Note that, in our case, $\mathcal{X}$ is the freespace $\mathcal{F}$, while f is the potential energy U.

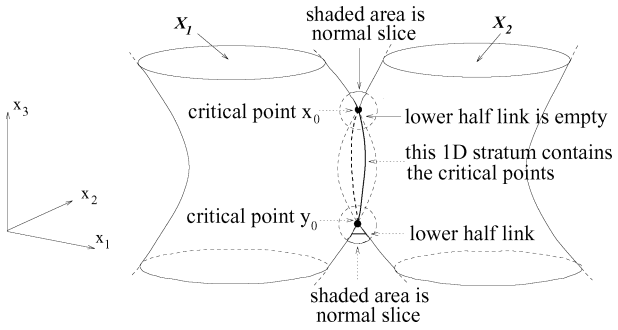

Fig. 3. Example showing the lower half link at the critical points x_0 and y_0. The function being used is $f(x_1, x_2, x_3) = x_3$.

The following proposition characterizes the local minima of f in $\mathcal{X}$.

Proposition 3.1: Let f be a Morse function on a regularly stratified set $\mathcal{X} \subset \mathbb{R}^m$, and let $x_0 \in \mathcal{X}$ be a critical point of f. Then, f has a *local minimum* at x_0 iff it satisfies the following two conditions

$$l^- = \emptyset \quad \text{and} \quad \sigma = 0 \tag{2}$$

where σ is the Morse index of f at x_0 and l^- is the lower half link of f at x_0.

A proof of the proposition appears in Appendix I. The condition $l^- = \emptyset$ is a "first derivative test," which verifies that f has a local minimum with respect to the neighboring strata at x_0. In our case, this condition verifies that U has a local minimum with respect to *contact breaking* motions of $\mathcal{B}$. The condition $\sigma = 0$ is the usual second-derivative test that ensures that f has a local minimum on the stratum containing x_0. In our case, this condition verifies that U has a local minimum with respect to *contact preserving* motions of $\mathcal{B}$.

Finally, it can be verified that, if x_0 is a local minimum of f in one c-space parametrization, it remains so in any other c-space parametrization. In our case, different parametrizations of c-space arise from different choices of world and body frames. The local minimum test (and subsequently the stability of the equilibrium point in question) is therefore independent of the reference frame choice.

IV. Characterization of Stable Stances

The stable equilibria of a mechanical system governed by a potential energy function are the *local minima* of this function [12], [38]. The stable equilibria of $\mathcal{B}$ are therefore the local minima of its potential energy function.[4] In order to adapt this principle to the evaluation of stance stability, we must express the local-minimum condition of SMT in terms of the geometry of $\mathcal{B}$ and the supporting bodies. We shall see that the condition $l^- = \emptyset$ depends on the contact normals, while the condition $\sigma = 0$ additionally depends on surface curvature at the contacts. This

[4]The stability principle assumes that c-space is a single smooth manifold, not a stratified set. It can be extended to stratified sets by adapting the stability result [36, Th. 1], which introduces compliance into the contact model.

section discusses the two conditions, summarizes the resulting stability test, then provides concrete formulas for the various terms in this test.

A. Testing for $l^- = \emptyset$

The following lemma gives a necessary and sufficient condition for l^- to be empty. In the lemma, $\tilde{f} : I\!R^m \to I\!R$ is a smooth function, and $f : \mathcal{F} \to I\!R$ is the restriction of $\tilde{f}$ to the freespace $\mathcal{F}$. Also recall that $\eta_i(q_0)$ is the unit normal to the ith c-obstacle boundary $\mathcal{S}_i$

Lemma 4.1 Let $f : \mathcal{F} \to I\!R$ be a smooth function. Let q_0 be a critical point of f on a stratum $\mathcal{S}$ of $\mathcal{F}$, such that $\mathcal{S}$ is the intersection of k c-obstacle boundaries, $\mathcal{S} = \cap_{i=1}^{k} \mathcal{S}_i$. A necessary condition for the lower half link at q_0, l^-, to be *empty* is

$$\nabla \tilde{f}(q_0) = \sum_{i=1}^{k} \lambda_i \eta_i(q_0) \tag{3}$$

for some scalars $\lambda_1, \ldots, \lambda_k$ such that $\lambda_i \geq 0$ for $i=1, \ldots, k$. Moreover, if the λ_i's are all strictly positive, (3) is also sufficient for $l^- = \emptyset$.

While a full proof appears in Appendix I, let us mention its key idea. If l^- is empty, f must be nondecreasing along all c-space paths $q(t)$ that start at q_0 and stay in $E(q_0) \cap \mathcal{F}$. Hence, $d/dt|_{t=0} f(q(t)) = \nabla \tilde{f}(q_0) \cdot \dot{q} \geq 0$ for all $\dot{q} \in E(q_0) \cap \mathcal{F}$. However, it is shown in the Appendix that only vectors $\eta \in N(q_0)$ satisfy this condition. Since $\nabla \tilde{f}(q_0)$ satisfies this condition too, it belongs to $N(q_0)$, which is condition (3).

In our case, the function f is the potential energy U, and the lemma provides the following geometric test for $l^- = \emptyset$. First, at an equilibrium q_0, we have that $\nabla U(q_0) = \sum_{i=1}^{k} \lambda_i \eta_i(q_0)$ where $\lambda_i \geq 0$ for $i = 1, \ldots, k$. Hence, the necessary condition (3) is automatically satisfied at an equilibrium. Thus, it suffices to check that all λ_i's in (3) are strictly positive. Equivalently, it suffices to check that $\nabla U(q_0)$ lies in the *interior* of the normal cone $N(q_0)$. The normal cone is spanned by the c-obstacle normals $\eta_1 \cdots \eta_k$, which can be expressed in terms of the geometric data. Let $\boldsymbol{\rho}_i$ be the vector from $\mathcal{B}$'s origin to the ith contact point, and let $\hat{l}_i$ be a unit vector collinear with the ith contact normal ($\hat{l}_i$ will be called the ith contact normal). Then, η_i is a positive multiple of the vector $(\hat{l}_i, \bar{\boldsymbol{\rho}}_i \times \hat{l}_i)$. Note that when $\nabla U(q_0)$ lies exactly on the boundary of $N(q_0)$ (i.e., when one of λ_i's vanishes), $U(q)$ fails to be Morse. In this case, it is not immediately known whether l^- is empty or not, as illustrated in the following example.

Example: Fig. 4 shows three different equilibrium stances of a planar object $\mathcal{B}$ supported by two bodies $\mathcal{A}_1$ and $\mathcal{A}_2$ against gravity. In Fig. 4(a), it can be inferred from the stance's symmetry that $\lambda_1 = \lambda_2 > 0$, and $l^- = \emptyset$ in this case. However, in Fig. 4(b) and (c), $\lambda_1 > 0$ while $\lambda_2 = 0$. Using methods discussed later, it can be shown that $l^- = \emptyset$ in Fig. 4(b) while $l^- \neq \emptyset$ in Fig. 4(c). This fact can be seen in the following intuitive way. Consider a rolling motion of $\mathcal{B}$ along $\mathcal{A}_1$ such that it breaks contact with $\mathcal{A}_2$. In Fig. 4(b), the height of $\mathcal{B}$'s center-of-mass increases during the rolling motion, suggesting that the original stance is a stable local minimum of U. In Fig. 4(c), the height of $\mathcal{B}$'s center-of-mass decreases during the rolling motion, indicating that the original stance is not a local minimum of U, and hence, unstable.

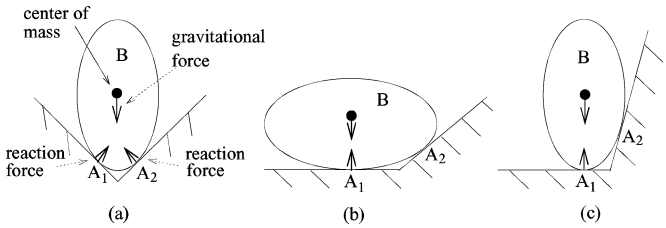

Fig. 4. Three different equilibrium stances. (a) $\lambda_1 = \lambda_2 > 0$ and $l^- = \emptyset$. (b) and (c) $\lambda_1 > 0$ but $\lambda_2 = 0$, and it is not immediately clear whether l^- is empty or not.

B. Testing for $\boldsymbol{\sigma} = 0$

The condition $\sigma = 0$ requires that q_0 be a local minimum of U on the stratum $\mathcal{S}$, where $\mathcal{S} = \cap_{i=1}^{k} \mathcal{S}_i$ is the stratum corresponding to contact with $\mathcal{A}_1, \ldots, \mathcal{A}_k$. The condition $\sigma = 0$ is trivially satisfied when the dimension of $\mathcal{S}$ is 0. Let us first characterize the cases where the dimension of $\mathcal{S}$, denoted by $\dim(\mathcal{S})$, is positive. In general, $\dim(\mathcal{S})$ is equal to the dimension of the ambient space m minus the dimension of the subspace spanned by the c-obstacle normals $\eta_1, \ldots, \eta_k$. Generically, the $m \times k$ matrix $[\eta_1 \cdots \eta_k]$ has full rank of $\min\{m, k\}$, and in this case, $\dim(\mathcal{S}) = m - \min\{m, k\}$. Hence, $\dim(\mathcal{S}) > 0$ when the number of contacts k satisfies $k < m$, and $\dim(\mathcal{S}) = 0$ when $k \geq m$. Thus, the test $\sigma = 0$ is generically required only for $1 \leq k < 3$ contacts in 2-D, and for $1 \leq k < 6$ contacts in 3-D. For a larger number of contacts, equilibrium automatically implies stability. However, many practically important cases involve $1 \leq k \leq m$ contacts, and this condition deserves careful consideration.

We now derive a geometric test for $\sigma = 0$, assuming $k < m$ contacts. For this number of contacts, the matrix $[\eta_1 \cdots \eta_k]$ has full rank iff the c-obstacle normals $\eta_1, \ldots, \eta_k$ are linearly independent. (Nongeneric cases such as when two contact-force lines coincide can be treated by extending the generic test derived later.) Let $q_0 \in \mathcal{S}$ be an equilibrium configuration of $\mathcal{B}$ under the influence of a potential energy U. Then, the condition $\sigma = 0$ is equivalent to the requirement that $d^2/dt^2\big|_{t=0} U(q(t)) > 0$ for all c-space paths $q(t)$ that start at q_0 and lie in the stratum $\mathcal{S}$. This condition involves both velocities and accelerations, since by application of the chain rule

$$\begin{aligned} \frac{d^2}{dt^2}\bigg|_{t=0} U(q(t)) &= \frac{d}{dt}\bigg|_{t=0} (\nabla U(q(t)) \cdot \dot{q}(t)) \\ &= \dot{q}^T D^2 U(q_0) \dot{q} + \nabla U(q_0) \cdot \ddot{q} \end{aligned} \tag{4}$$

where $\dot{q} = \dot{q}(0)$ and $\ddot{q} = \ddot{q}(0)$. Since $\mathcal{S} = \cap_{i=1}^{k} \mathcal{S}_i$, any c-space path $q(t)$ in $\mathcal{S}$ must, in particular, lie in each $\mathcal{S}_i$ for $i = 1, \ldots, k$. It follows that $\ddot{q}$ in (4) depends on the curvature of the c-obstacle boundaries $\mathcal{S}_1, \ldots, \mathcal{S}_k$. These curvatures depend in turn on the curvature of the contacting bodies. The curvature of $\mathcal{S}_i$ at $q \in \mathcal{S}_i$ measures the change in the normal $\eta_i(q)$ along the direction $\dot{q}$, and is given by $\kappa_i(q, \dot{q}) = \dot{q}^T D\eta_i(q) \dot{q}$. The following weighted

sum gives the desired geometric test for $\sigma = 0$, as shown in the proposition later.

Defination 1: Let $\mathcal{B}$ be at an equilibrium configuration q_0, under the influence of a potential energy U, such that $\mathcal{B}$ is supported by k bodies $\mathcal{A}_1, \ldots, \mathcal{A}_k$ where $k < m$. The *relative curvature form* associated with U is

$$\kappa_U(q_0, \dot{q}) = \sum_{i=1}^{k} \lambda_i \kappa_i(q_0, \dot{q}) - \dot{q}^T D^2U(q_0)\dot{q}, \qquad \dot{\mathrm{q}} \in \mathrm{T}_{\mathrm{q}_0}\mathcal{S} \tag{5}$$

where the λ_i's are the equilibrium-condition coefficients, $\kappa_i(q_0, \dot{q})$ is the curvature of $\mathcal{S}_i$ at q_0, and $\mathcal{S} = \cap_{i=1}^{k} \mathcal{S}_i$.

In particular, the relative curvature form associated with the gravitational potential energy is called the *gravity relative curvature form*, and is denoted as $\kappa_G(q_0, \dot{q})$.

The scalars $\lambda_1, \ldots, \lambda_k$ are determined by the equilibrium equation: $\nabla U(q_0) = \sum_{i=1}^{k} \lambda_i \eta_i(q_0)$. These scalars are uniquely determined in the generic case where $\eta_1, \ldots, \eta_k$ are linearly independent. Thus, $\kappa_U(q_0, \dot{q})$ is well defined. The following proposition relates the relative curvature form $\kappa_U(q_0, \dot{q})$ to the condition $\sigma = 0$.

Proposition 4.2: Let U be a potential energy function that is Morse on $\mathcal{F}$. Let $\mathcal{B}$ be at an equilibrium configuration q_0, supported by k bodies $\mathcal{A}_1, \ldots, \mathcal{A}_k$ where $k < m$. Then, $\sigma = 0$ iff the relative curvature form associated with U is negative definite

$$\sigma = 0 \text{ iff } \kappa_U(q_0, \dot{q}) < 0 \qquad \text{for all } \dot{q} \in T_{q_0}\mathcal{S}$$

where $\mathcal{S} = \cap_{i=1}^{k} \mathcal{S}_i$.

Proof: Let $q(t)$ be a c-space trajectory which starts at q_0 and lies in the stratum $\mathcal{S}$, with $\dot{q} = \dot{q}(0)$ and $\ddot{q} = \ddot{q}(0)$. Since $q(t)$ lies in $\mathcal{S}$, its tangent vector $\dot{q}(t)$ satisfies $\eta_i(q(t)) \cdot \dot{q}(t) = 0$ for all t. Taking the derivative of this expression, we find

$$\eta_i(q(t)) \cdot \ddot{q}(t) + \dot{q}^T(t) D\eta_i(q(t))\dot{q}(t) = 0 \qquad \text{for all } t. \tag{6}$$

Next consider the second derivative of $U(q(t))$ at $t = 0$ specified in (4). In this equation, $\nabla U(q_0) = \sum_{i=1}^{k} \lambda_i \eta_i(q_0)$ at the equilibrium q_0. Hence, $d^2/dt^2|_{t=0} U(q(t)) = \dot{q}^T D^2U(q_0)\dot{q} + \sum_{i=1}^{k} \lambda_i \eta_i(q_0) \cdot \ddot{q}$. Substituting for $\eta_i(q_0) \cdot \ddot{q}$ according to (6) gives

$$\left.\frac{d^2}{dt^2}\right|_{t=0} U(q(t)) = \dot{q}^T (D^2U(q_0) - \sum_{i=1}^{k} \lambda_i D\eta_i(q_0)\dot{q})$$
$$= -\kappa_U(q_0, \dot{q}).$$

Thus, U increases along $q(t)$ if and only if $\kappa_U(q_0, \dot{q}) < 0$, where $\dot{q} = \dot{q}(0)$. The latter result holds for all c-space paths that start at q_0 and lie in $\mathcal{S}$. Since $T_{q_0}\mathcal{S}$ is the collection of tangents at q_0 to these paths, we obtain the condition $\kappa_U(q_0, \dot{q}) < 0$ for all $\dot{q} \in T_{q_0}\mathcal{S}$.

C. Summary of Stance Stability Test

We now summarize the stance stability test in terms of the contacting bodies' geometry. However, the test requires that U be Morse at the equilibrium point. In order to characterize this Morse condition, let $q_0 \in \mathcal{S}$ be an equilibrium point of $\mathcal{B}$. Then the function U can fail to be Morse at q_0 in one of two ways. First, U is not Morse at q_0 if $\nabla U(q_0)$ is normal to any of the other strata meeting at q_0. It also fails to be Morse if $D^2U(q_0)$, evaluated along $\mathcal{S}$, has zero eigenvalues. The latter condition implies that a third-order derivative is required to determine stability. The following lemma provides a test for the two conditions. The interior of the normal cone $N(q_0)$ is the collection of vectors $\lambda_1\eta_1(q_0) + \cdots + \lambda_k\eta_k(q_0)$ such that λ_i's are all strictly positive.

Lemma 4.3: Let $q_0 \in \mathcal{S}$ be an equilibrium configuration of $\mathcal{B}$, where $\mathcal{S} = \cap_{i=1}^{k} \mathcal{S}_i$. Then U is *Morse* at q_0 if $\nabla U(q_0)$ lies in the interior of the normal cone $N(q_0)$, and if the eigenvalues of the matrix of $\kappa_U(q_0, \dot{q})$, which is $\sum_{i=1}^{k} \lambda_i D\eta_i(q_0) - D^2U(q_0)$, are nonzero.

The lemma is proved in Appendix I. We can now summarize the stance stability test.

Theorem 1: Stance stability test: Let a rigid object $\mathcal{B}$ be at an equilibrium configuration q_0, supported by bodies $\mathcal{A}_1, \ldots, \mathcal{A}_k$ under the influence of a potential energy U. Let the matrix $[\eta_1 \cdots \eta_k]$ of c-obstacle normals have full rank (which is the generic case). Let $m = 3$ or 6 be $\mathcal{B}$'s c-space dimension.

For $k \geq m$ contacts, the equilibrium is locally *stable* if there exists a subcollection of m linearly independent c-obstacle normals such that

$$\nabla U(q_0) \in \mathsf{interior}(N'(q_0)) \tag{7}$$

where $N'(q_0)$ is the cone spanned by these normals.

For $k < m$ contacts, the equilibrium is locally *stable* if first

$$\nabla U(q_0) \in \mathsf{interior}(N(q_0)) \tag{8}$$

where $N(q_0)$ is the normal cone at q_0. And second, if

$$\kappa_U(q_0, \dot{q}) < 0 \qquad \text{for all } \dot{\mathrm{q}} \in \mathrm{T}_{\mathrm{q}_0}\mathcal{S} \tag{9}$$

where $\kappa_U(q_0, \dot{q})$ is the relative curvature form associated with U, and $\mathcal{S} = \cap_{i=1}^{k} \mathcal{S}_i$.

Proof: Since conditions (7)–(9) guarantee that U is Morse at q_0 according to Lemma 4.3, we may invoke the SMT condition for a local minimum. For clarity, let us focus on the cases where $k \leq m$. According to Proposition 3.1, q_0 is a local minimum of U if $l^- = \emptyset$ and $\sigma = 0$. Lemma 4.1 asserts that $l^- = \emptyset$ whenever λ_i's in the equation $\nabla U(q_0) = \sum_{i=1}^{k} \lambda_i \eta_i$ are all positive. Condition (8) specifies that $\nabla U(q_0)$ lies in the interior of $N(q_0)$, which implies that λ_i's are all positive. Thus, $l^- = \emptyset$. Proposition 4.2 asserts that $\sigma = 0$ whenever (9) holds true. Thus, q_0 is a local minimum of U and is therefore stable.

Physical interpretation of stability test: The relative curvature form verifies that q_0 is a local minimum of U on the stratum $\mathcal{S}$, and condition (9) corresponds to a classical second-derivative test. This test is not required for $k \geq m$ contacts, since $\mathcal{S}$ is zero-dimensional in this case. The stratum $\mathcal{S}$ corresponds to motions where $\mathcal{B}$ maintains contact with all k bodies. However, one must also consider the possibility that $\mathcal{B}$ may break contact with some of the supporting bodies. The test specified in (8) (for $k < m$ contacts) or (7) (for $k \geq m$ contacts) ensures that U has a local minimum with respect to such contact-breaking motions.

Finally, consider the stability of an equilibrium q_0 when $\nabla U(q_0)$ lies on the boundary of $N(q_0)$. In this case, one or more of the λ_i's in the equilibrium equation vanishes. The corresponding contacts generate zero reaction force and are therefore nonactive. For stability analysis, we may ignore these contacts and evaluate $\kappa_U(q_0, \dot{q})$ on the stratum $\mathcal{S}$ corresponding to the active contacts. If the equilibrium is stable, adding back the nonactive contacts would not destroy stability.

D. Formulas for Stability Test Terms

We now list concrete formulas for the terms in the stability test of Theorem I. Let $\boldsymbol{r}_{\rm cm}$ be the location of $\mathcal{B}$'s center-of-mass expressed in its body frame. The world coordinates of $\mathcal{B}$'s center-of-mass, denoted by $x_{\rm cm}$, are given by $x_{\rm cm}(q) = R(\theta)\boldsymbol{r}_{\rm cm} + d$, where $q = (d, \theta)$ is $\mathcal{B}$'s configuration. Tangent vectors in this representation are pairs $\dot{q} = (v, \omega)$, where v and ω are $\mathcal{B}$'s linear and angular velocities. When $\mathcal{B}$ is at a configuration q, the vector from $\mathcal{B}$'s origin to $x_{\rm cm}$, denoted by $\boldsymbol{\rho}_{\rm cm}$, is given by $\boldsymbol{\rho}_{\rm cm}(\theta) = R(\theta)\boldsymbol{r}_{\rm cm}$. The term $[a\times]$ denotes the 3×3 cross-product matrix satisfying $[a\times]b = a \times b$ for all $a, b \in I\!R^3$.

Lemma 4.4: (Formulas for U, ∇U, D^2U): The gravitational potential energy of a 3-D object $\mathcal{B}$ is given by

$$U(q) = mg(\boldsymbol{e} \cdot \boldsymbol{x}_{\rm cm}(q))$$

where m is $\mathcal{B}$'s mass, g the gravity constant, and $e = (0, 0, 1)$ the vertical upward direction. The gradient of U is given by

$$\nabla U(q) = mg \begin{pmatrix} \boldsymbol{e} \\ \boldsymbol{\rho}_{\rm cm}(\theta) \times \boldsymbol{e} \end{pmatrix} \tag{10}$$

where $\boldsymbol{\rho}_{\rm cm}(\theta) \times e = (y_{\rm cm}, -x_{\rm cm}, 0)$ using the coordinates $\boldsymbol{\rho}_{\rm cm} = (x_{\rm cm}, y_{\rm cm}, z_{\rm cm})$. The second derivative matrix of U is given by

$$D^2U(q) = mg \begin{bmatrix} O & O \\ O & ([\boldsymbol{\rho}_{\rm cm}(\theta)\times][\boldsymbol{e}\times])_s \end{bmatrix} \tag{11}$$

where O is a 3×3 matrix of zeroes, and $A_s = 1/2(A + A^T)$.

The formulas for ∇U and D^2U in the 2-D case can be derived from (10) and (11) as follows. Let $\boldsymbol{u}_1 \times \boldsymbol{u}_2$ be defined as the scalar $\boldsymbol{u}_1 \times \boldsymbol{u}_2 = \det[\boldsymbol{u}_1\ \boldsymbol{u}_2]$ where $\boldsymbol{u}_1, \boldsymbol{u}_2 \in I\!R^2$.

Corollary 4.5: Let $\mathcal{B}$ be a 2-D object in a planar gravitational environment, with $e = (0, 1)$ the vertical upward direction. Then, ∇U is given by

$$\nabla U(q) = mg \begin{pmatrix} \boldsymbol{e} \\ \boldsymbol{\rho}_{\rm cm}(\theta) \times \boldsymbol{e} \end{pmatrix} = mg \begin{pmatrix} \boldsymbol{e} \\ \boldsymbol{x}_{\rm cm} \end{pmatrix} \tag{12}$$

where $\boldsymbol{\rho}_{\rm cm} = (x_{\rm cm}, y_{\rm cm})$. The formula for D^2U is

$$D^2U(q) = -mg \begin{bmatrix} O & 0 \\ 0^T & \boldsymbol{\rho}_{\rm cm}(\theta) \cdot e \end{bmatrix} = -mg \begin{bmatrix} O & 0 \\ 0^T & y_{\rm cm} \end{bmatrix} \tag{13}$$

where O is a 2×2 matrix of zeroes.

A derivation of these formulas appears in [21]. Next we give a formula for the c-obstacle normal $\eta_i(q)$. When $\mathcal{B}$ is at a configuration $q \in \mathcal{S}_i$, it contacts $\mathcal{A}_i$ at a point $x_i = R(\theta)r_i + d$ where r_i is the contact point expressed in $\mathcal{B}$'s body frame. Let $\boldsymbol{\rho}_i(\theta) = R(\theta)r_i$, and let $\hat{l}_i$ be the unit contact normal at x_i. Using the virtual work principle, it can be shown that $\eta_i(q) = 1/c_i(\hat{l}_i, \boldsymbol{\rho}_i \times \hat{l}_i)$, where $c_i = \sqrt{1 + ||\boldsymbol{\rho}_i \times \hat{l}_i{}^2||}$.

The last formula is for the c-obstacle curvature forms, $\kappa_i(q, \dot{q})$ for $i = 1 \ldots k$. The formula for the 3-D case appears in [34]. The formula for the 2-D case, used in Section V, is as follows. Let $\kappa_{\mathcal{B}_i}$ and $\kappa_{\mathcal{A}_i}$ be the scalar curvatures of the curves bounding $\mathcal{B}(q)$ and $\mathcal{A}_i$ at x_i. The curvature of a convex curve is positive, that of a concave curve is negative. Recall that every $\dot{q} \in T_q\mathcal{S}_i$ corresponds to an instantaneous rotation of $\mathcal{B}$ about some point along the line l_i. Thus, we give a formula for $\kappa_i(q, \dot{q})$ along instantaneous rotations $\dot{q} = (0, \omega)$ such that $\mathcal{B}$'s origin sweeps the line l_i. Let the scalar ρ_i denote the distance of $\mathcal{B}$'s origin from the ith contact, where ρ_i is positive on $\mathcal{B}$'s side of the contact and negative on $\mathcal{A}_i$'s side.

Corollary 4.6: [34] Let $\mathcal{B}$ and $\mathcal{A}_i$ be planar bodies. The c-space curvature of $\mathcal{S}_i$ at $q \in \mathcal{S}_i$ along instantaneous rotation $\dot{q} = (0, \omega)$ of $\mathcal{B}$ about an axis located at a distance ρ_i along l_i is

$$\kappa_i(q, (0, \omega)) = \frac{(\rho_i\kappa_{\mathcal{B}_i} - 1)(\rho_i\kappa_{\mathcal{A}_i} + 1)}{\kappa_{\mathcal{A}_i} + \kappa_{\mathcal{B}_i}}\omega^2 \tag{14}$$

where ω is a scalar. The curvature of $\mathcal{S}_i$ along instantaneous translation $\dot{q} = (v, 0)$ of $\mathcal{B}$ is

$$\kappa_i(q, (v, 0)) = \frac{1}{c_i} \cdot \frac{\kappa_{\mathcal{A}_i}\kappa_{\mathcal{B}_i}}{\kappa_{\mathcal{A}_i} + \kappa_{\mathcal{B}_i}}\|v^2\| \tag{15}$$

where $c_i = \sqrt{1 + ||\boldsymbol{\rho}_i \times \hat{l}_i{}^2||}$.

The denominator in (14) and (15) always satisfies $\kappa_{\mathcal{A}_i} + \kappa_{\mathcal{B}_i} \geq 0$, since $\kappa_{\mathcal{A}_i} + \kappa_{\mathcal{B}_i} < 0$ would imply that the two bodies penetrate each other. Moreover, $\kappa_{\mathcal{A}_i} + \kappa_{\mathcal{B}_i} > 0$ in the generic case where the bodies' circles of curvature maintain point contact.

Remark: Let $r_{\mathcal{A}_i} = 1/\kappa_{\mathcal{A}_i}$ and $r_{\mathcal{B}_i} = 1/\kappa_{\mathcal{B}_i}$ be the radii-of-curvature of $\mathcal{A}_i$ and $\mathcal{B}$ at x_i. Then, (14) can be written as

$$\kappa_i(q, (0, \omega)) = \frac{(\rho_i - r_{\mathcal{B}_i})(\rho_i + r_{\mathcal{A}_i})}{r_{\mathcal{A}_i} + r_{\mathcal{B}_i}}\omega^2. \tag{16}$$

Since $T_q\mathcal{S}_i$ corresponds to instantaneous rotations of $\mathcal{B}$ about points on the line l_i, the sign of $\kappa_i(q, \dot{q})$ for all $\dot{q} \in T_q\mathcal{S}_i$ can be determined by evaluating (16) using $\omega = 1$ and $-\infty \leq \rho_i \leq \infty$.

V. Stable Equilibrium Region of Planar Stances

This section applies the stance stability test to the following problem (which is used later for quasi-static locomotion synthesis). A planar object $\mathcal{B}$ is supported by k frictionless contacts against gravity. We wish to characterize the set of $\mathcal{B}$'s center-of-mass positions guaranteeing stable equilibrium, assuming that the contacts are held fixed. We begin with a generic computation of the stable center-of-mass locations, then analyze the various k-contact stances.

A. Computation of $\mathcal{E}(q_0)$ and $\mathcal{E}^S(q_0)$

Let the *equilibrium region*, denoted as $\mathcal{E}(q_0)$, be the set of $\mathcal{B}$'s center-of-mass positions guaranteeing static equilibrium. Let the *stability region*, denoted by $\mathcal{E}^S(q_0)$, be the subset of $\mathcal{E}(q_0)$ guaranteeing stable equilibrium. Consider now a planar gravitational environment whose vertical upward direction is $\boldsymbol{e} = (0, 1)$. Using Corollary 4.5, the gravitational wrench acting

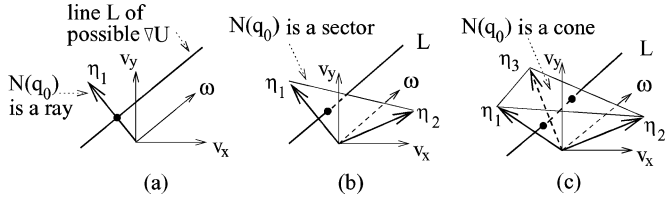

Fig. 5. Line L of possible $\nabla U(q_0)$ and the normal cone $N(q_0)$, shown in $T_{q_0}I\!R^3$. (a) For a single contact, $L \cap N(q_0)$ is at most at a single point. (b) For two contacts, $L \cap N(q_0)$ is generically a single point. (c) For three contacts, $L \cap N(q_0)$ is generically an interval.

on $\mathcal{B}(q)$ is

$$\nabla U(q) = mg\begin{pmatrix} \boldsymbol{e} \\ x_{\rm cm} \end{pmatrix} = mg\left\{ \begin{pmatrix} 0 \\ 1 \\ 0 \end{pmatrix} + \mathrm{x_{cm}} \begin{pmatrix} 0 \\ 0 \\ 1 \end{pmatrix} \right\} \qquad (17)$$

where $x_{\rm cm}$ is the horizontal coordinate of $\mathcal{B}$'s center-of-mass. Since $x_{\rm cm}$ is a free parameter, (17) implies that the collection of possible gravitational wrenches forms an affine line in $T_q I\!R^3$ (recall that ∇U is treated as a tangent vector in $T_q I\!R^3$). Let L denote this line, and let (v_x, v_y, ω) be the coordinates of $T_q I\!R^3$. Then L is perpendicular to the (v_x, v_y)-plane and passes through the point $(\boldsymbol{e}, 0) \in T_q I\!R^3$ (Fig. 5). When $\mathcal{B}$ lies at a k-contact equilibrium configuration q_0, $\nabla U(q_0) \in N(q_0)$. Hence, every point where L intersects $N(q_0)$ determines a value of $x_{\rm cm}$ that is a feasible equilibrium stance of $\mathcal{B}$ associated with the k contacts. Each such value of $x_{\rm cm}$ determines a *vertical line* in the physical environment that belongs to the equilibrium region $\mathcal{E}(q_0)$. Since $N(q_0)$ is convex, the intersection of L with $N(q_0)$, if nonempty, is convex and connected. When L intersects $N(q_0)$ at a single point [see Fig. 5(a) and Fig. 5(b)], $\mathcal{E}(q_0)$ is a single vertical line. When L intersects $N(q_0)$ along a finite interval (see Fig. 5(c)), $\mathcal{E}(q_0)$ is a vertical strip. The intersection may also occur along a semi-infinite interval, and in this case, $\mathcal{E}(q_0)$ is a vertical half-plane.

We now derive a geometric test for checking that L intersects $N(q_0)$. First we scale the gravitational gradient so that $mg = 1$ (this scaling amounts to a choice of energy units). Let V denote the (v_x, v_y)-plane in $T_{q_0} I\!R^3$, corresponding to linear velocities of $\mathcal{B}$. Since L is orthogonal to V, L intersects $N(q_0)$ iff the projections of L and $N(q_0)$ onto V intersect each other. The projection of L is the point $\boldsymbol{e} = (0, 1)$. Since $N(q_0)$ is spanned by the c-obstacle normals $\eta_1(q_0) \cdots \eta_k(q_0)$, its projection on V is the positive span of the projection of these normals. The projection of η_i onto V is a positive multiple of the ith contact normal $\hat{l}_i$. Thus, *L intersects $N(q_0)$ iff $\boldsymbol{e}$ lies in the positive span of the contact normals* $\hat{l}_1, \ldots, \hat{l}_k$. If $\boldsymbol{e}$ is positively spanned by the $\hat{l}_i$'s, there must be some choice(s) of $x_{\rm cm}$ such that ∇U lies inside $N(q_0)$, and the equilibrium region is nonempty. If $\boldsymbol{e}$ does not lie in the positive span of $\hat{l}_i$'s, no equilibrium is possible for any location of $\mathcal{B}$'s center-of-mass. This is summarized in the following proposition.

Proposition 5.1: Let a planar object $\mathcal{B}$ be supported by k frictionless contacts against gravity. Then the *equilibrium region* of $\mathcal{B}$ is nonempty iff the contact normals $\hat{l}_1, \ldots, \hat{l}_k$ positively span the upward vertical direction $\boldsymbol{e}$.

TABLE 1
SUMMARY OF STABILITY RESULTS FOR A SINGLE-CONTACT STANCE

Support	Object		Stability
convex	convex	$\kappa_{A_1} > 0,\ \kappa_{B_1} > 0$	always unstable
concave	convex	$\kappa_{A_1} < 0,\ \kappa_{B_1} > 0$	stable iff $s_{cm} < (1/\kappa_{B_1})$
convex	concave	$\kappa_{A_1} > 0,\ \kappa_{B_1} < 0$	stable iff $s_{cm} < (1/\kappa_{B_1})$
convex	flat	$\kappa_{A_1} > 0,\ \kappa_{B_1} = 0$	always unstable
flat	convex	$\kappa_{A_1} = 0,\ \kappa_{B_1} > 0$	neutrally stable under pure translation otherwise stable iff $s_{cm} < (1/\kappa_{B_1})$

Moreover, if the equilibrium region is nonempty, it is generically a single vertical line for $k = 1, 2$ contacts, and a vertical strip or half-plane for $k \geq 3$ contacts.

The curvature part of the stability test (9) can be expressed in a more convenient form as follows. Using (13) and (14) for the terms in $\kappa_G(q_0, \dot{q})$, we find that the angular velocity ω appears quadratically in $\kappa_G(q_0, \dot{q})$. Hence, we may substitute $\omega = 1$ without affecting the sign of $\kappa_G(q_0, \dot{q})$. This substitution gives the following stability condition

$$\kappa_G \stackrel{\triangle}{=} \boldsymbol{\rho}_{\rm cm} \cdot \boldsymbol{e} + \sum_{\rm i=1}^{\rm k} \lambda_{\rm i} \frac{(\rho_{\rm i}\kappa_{\rm B_i} - 1)(\rho_{\rm i}\kappa_{\rm A_i} + 1)}{\kappa_{\rm A_i} + \kappa_{\rm B_i}} < 0. \qquad (18)$$

In this formula, tangent vectors in $T_{q_0}\mathcal{S}$ are parametrized by ρ_i, the signed distance of $\mathcal{B}$'s origin from the ith contact, while $\boldsymbol{\rho}_{\rm cm}$ is the vector from $\mathcal{B}$'s origin to its center-of-mass. Next, we determine the stable equilibrium region of the various k-contact stances.

B. Single Contact Stances

A single-contact stance must have $\hat{l}_1 = \boldsymbol{e}$ for an equilibrium to exist. In this case, the equilibrium region $\mathcal{E}(q_0)$ is the entire line l_1. Since $\mathcal{B}$'s center-of-mass lies on the vertical line l_1, the vector $\boldsymbol{\rho}_{\rm cm} = (x_{\rm cm}, y_{\rm cm})$ is collinear with $\boldsymbol{e}$. Hence, $\boldsymbol{\rho}_{\rm cm} \cdot \boldsymbol{e} = y_{\rm cm}$ in (18), and the stability test is

$$\kappa_G = y_{\rm cm} + \frac{(\rho_1\kappa_{\mathcal{B}_1} - 1)(\rho_1\kappa_{\mathcal{A}_1} + 1)}{\kappa_{\mathcal{A}_1} + \kappa_{\mathcal{B}_1}} < 0, \qquad (19)$$

for $-\infty \leq \rho_1 \leq \infty$.

The resulting κ_G is linear in $y_{\rm cm}$; hence $\mathcal{E}^S(q_0)$ is a *lower half-line* of l_1. It is now a matter of elementary algebra to determine which values of $y_{\rm cm}$ guarantee that κ_G is negative for all ρ_1; see Table I for a summary of the possible cases. In particular, the case where $\mathcal{B}$ rests on a horizontal plane is well known (e.g., [13]). In this case, the condition $\kappa_G < 0$ for all ρ_1 gives that $\mathcal{B}$'s center-of-mass must lie below its center-of-curvature for stability.

C. Two Contact Stances

For two contacts, Proposition 5.1 implies that $\boldsymbol{e}$ must lie in the positive span of $\hat{l}_1$ and $\hat{l}_2$ for an equilibrium to exist. If this condition is satisfied, we must consider the possible intersection arrangements of L with $N(q_0)$. If $\hat{l}_1$ and $\hat{l}_2$ are nonparallel, L intersects $N(q_0)$ at a point [see Fig. 5(b)]. The intersection corresponds to $\mathcal{B}$'s center-of-mass lying on the vertical line passing through the intersection point of l_1 and l_2. Let p denote this intersection point. Then $\mathcal{E}(q_0)$ is the *single vertical line*, denoted by l', that passes through p (Fig. 6). If $\hat{l}_1$ and $\hat{l}_2$ are parallel, they

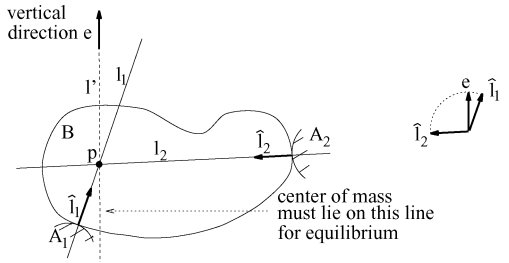

Fig. 6. Two-contact equilibrium stance where l_1 and l_2 intersect at p.

must be vertical for an equilibrium to exist. Moreover, either $\hat{l}_1 = \hat{l}_2$ or $\hat{l}_1 = -\hat{l}_2$ (we assume that l_1 and l_2 do not coincide). In this case, L intersects $N(q_0)$ in a finite or semi-infinite interval. If $\hat{l}_1 = \hat{l}_2 = e$, L intersects $N(q_0)$ along a finite-width interval, and the equilibrium region is the *vertical strip* bounded by l_1 and l_2. If $\hat{l}_1 = e$ say, but $\hat{l}_2 = -e$, L intersects $N(q_0)$ along a semi-infinite interval. In this case, $\mathcal{E}(q_0)$ is the *vertical half-plane* bounded by l_1, which does not contain l_2.

Next we identify the stability region $\mathcal{E}^S(q_0)$. For stability, κ_G must be negative for all motions $\dot{q} \in T_{q_0}\mathcal{S}$, where $\mathcal{S} = \mathcal{S}_1 \cap \mathcal{S}_2$. When l_1 and l_2 intersect at a point p, the tangent space $T_{q_0}\mathcal{S}$ consists of instantaneous rotations of $\mathcal{B}$ about p. Hence, κ_G in (18) must be evaluated at a value of ρ_i that is the distance of p from the ith contact ($i = 1, 2$). Let $\mathcal{B}$'s origin be located at p. Since $\mathcal{B}$'s center-of-mass lies on the vertical line l', the vector $\boldsymbol{\rho}_{\rm cm} = (x_{\rm cm}, y_{\rm cm})$ is collinear with $\boldsymbol{e}$. Hence, $\boldsymbol{\rho}_{\rm cm} \cdot \boldsymbol{e} = y_{\rm cm}$ in (18). The stability test is then

$$\kappa_G = y_{\rm cm} + \lambda_1 \frac{(\rho_1\kappa_{\mathcal{B}_1} - 1)(\rho_1\kappa_{\mathcal{A}_1} + 1)}{\kappa_{\mathcal{A}_1} + \kappa_{\mathcal{B}_1}} + \lambda_2 \frac{(\rho_2\kappa_{\mathcal{B}_2} - 1)(\rho_2\kappa_{\mathcal{A}_2} + 1)}{\kappa_{\mathcal{A}_2} + \kappa_{\mathcal{B}_2}} < 0. \quad (20)$$

The coefficients λ_1 and λ_2 are determined by the equation $\lambda_1\hat{l}_1 + \lambda_2\hat{l}_2 = \boldsymbol{e}$ as follows. Let α_1 and α_2 be the angles between $\hat{l}_1$ and $\hat{l}_2$ and the vertical line l' (Fig. 7). Taking the vector cross-product of both sides of the equation $\lambda_1\hat{l}_1 + \lambda_2\hat{l}_2 = \boldsymbol{e}$ with $\hat{l}_2$ and $\hat{l}_1$, then solving for λ_1 and λ_2 gives

$$\lambda_1\hat{l}_1 \times \hat{l}_2 = \boldsymbol{e} \times \hat{l}_2 \Rightarrow \lambda_1 = \frac{\boldsymbol{e} \times \hat{l}_2}{\hat{l}_1 \times \hat{l}_2} = \frac{\sin\alpha_2}{\sin(\alpha_1+\alpha_2)}$$

$$\lambda_2\hat{l}_2 \times \hat{l}_1 = \boldsymbol{e} \times \hat{l}_1 \Rightarrow \lambda_2 = \frac{\boldsymbol{e} \times \hat{l}_1}{\hat{l}_2 \times \hat{l}_1} = \frac{\sin\alpha_1}{\sin(\alpha_1+\alpha_2)}. \quad (21)$$

Moreover, it can be verified that $\sin\alpha_1$, $\sin\alpha_2$, and $\sin(\alpha_1+\alpha_2)$ are all positive at the equilibrium. Substituting for λ_1 and λ_2 in (20) gives

$$\kappa_G = y_{\rm cm} + \frac{\sin\alpha_2}{\sin(\alpha_1+\alpha_2)} \frac{(\rho_1\kappa_{\mathcal{B}_1} - 1)(\rho_1\kappa_{\mathcal{A}_1} + 1)}{\kappa_{\mathcal{A}_1} + \kappa_{\mathcal{B}_1}} + \frac{\sin\alpha_1}{\sin(\alpha_1+\alpha_2)} \frac{(\rho_2\kappa_{\mathcal{B}_2} - 1)(\rho_2\kappa_{\mathcal{A}_2} + 1)}{\kappa_{\mathcal{A}_2} + \kappa_{\mathcal{B}_2}} < 0. \quad (22)$$

Note that all terms in (22) are explicit functions of the geometric data. Since κ_G is linear in $y_{\rm cm}$, the stable equilibrium region

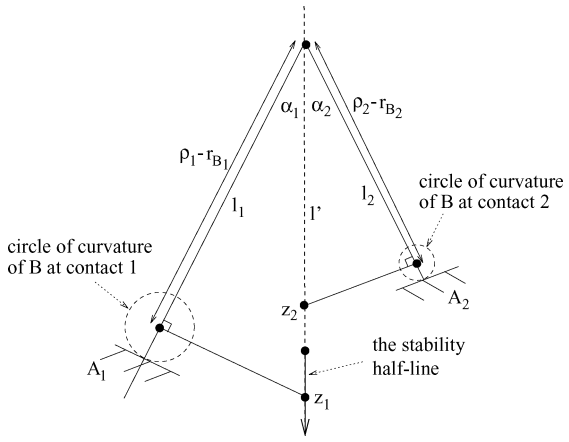

Fig. 7. Stability lower half-line for two flat supports.

$\mathcal{E}^S(q_0)$ is a *lower half-line of* l'. We now discuss a special case that yields a graphical interpretation of the formula.

Graphically determinable special case: Consider a stance with two flat supports, i.e., $\kappa_{\mathcal{A}_i} = 0$ for $i = 1, 2$. Substituting $\kappa_{\mathcal{A}_i} = 0$ and $\kappa_{\mathcal{B}_i} = 1/r_{\mathcal{B}_i}$ in (22) and factoring gives

$$\kappa_G = \sum_{i=1}^{2} \frac{\sin(\alpha_{i+1})}{\sin(\alpha_1+\alpha_2)} (y_{\rm cm}\cos\alpha_i + (\rho_i - r_{\mathcal{B}_i})) < 0 \quad (23)$$

where index addition is taken modulus 2. Condition (23) admits the following interpretation. Let z_i be the intersection point of the vertical line l' with the line perpendicular to l_i which passes through $\mathcal{B}$'s center-of-curvature at the ith contact (Fig. 7). Then the ith summand in (23) is negative when $\mathcal{B}$'s center-of-mass lies below z_i, zero when it lies at z_i, and positive when it lies above z_i. The resulting stability half-line lies below the point $z_1 + \sin\alpha_1 \cos\alpha_2 / \sin(\alpha_1+\alpha_2)(z_2 - z_1)$, which is at the midpoint between z_1 and z_2 when $\alpha_1 = \alpha_2$. The example provides an important insight for locomotion synthesis: $\mathcal{B}$ can raise its stability half-line by using lower curvature at the contacts. This observation holds for general two-contact stances.

Last consider $\mathcal{E}^S(q_0)$ in the case where $\hat{l}_1$ and $\hat{l}_2$ are parallel. Recall that, in this case, $\mathcal{E}(q_0)$ is either a vertical strip or a vertical half-plane. The tangent space $T_{q_0}\mathcal{S}$ consists of instantaneous translations of $\mathcal{B}$ in the direction perpendicular to $\hat{l}_1$ and $\hat{l}_2$. Substituting for κ_1 and κ_2 according to (15) gives the stability test

$$\kappa_G = \lambda_1\kappa_1 + \lambda_2\kappa_2 = \frac{\lambda_1}{c_1} \cdot \frac{\kappa_{\mathcal{A}_1}\kappa_{\mathcal{B}_1}}{\kappa_{\mathcal{A}_1} + \kappa_{\mathcal{B}_1}} + \frac{\lambda_2}{c_2} \cdot \frac{\kappa_{\mathcal{A}_2}\kappa_{\mathcal{B}_2}}{\kappa_{\mathcal{A}_2} + \kappa_{\mathcal{B}_2}} < 0 \quad (24)$$

where λ_1 and λ_2 are determined by the equilibrium condition. Since $\lambda_1, \lambda_2 \geq 0$, the sign of κ_G depends on the sign of κ_1 and κ_2. Each κ_i is positive when $\mathcal{B}$ and $\mathcal{A}_i$ are convex at the ith contact, zero if either boundary is flat, and negative otherwise. When κ_1 and κ_2 are both negative, $\mathcal{E}^S(q_0) = \mathcal{E}(q_0)$; when κ_1 and κ_2 are both positive, $\mathcal{E}^S(q_0)$ is empty. Finally, when κ_1 and κ_2 have mixed signs, $\mathcal{E}^S(q_0)$ is a substrip of $\mathcal{E}(q_0)$, whose formula appears in [21].

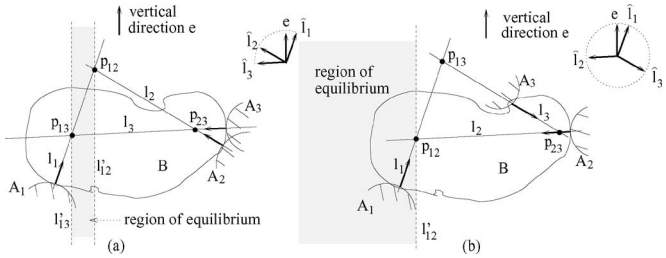

Fig. 8. Three-contact stances where $\hat{l}_1, \hat{l}_2, \hat{l}_3$ span positively. (a) Portion of the plane. and (b) Entire plane.

D. Stances Involving Three or More Contacts

For three-contact stances, almost any placement of $\mathcal{B}$'s center-of-mass in $\mathcal{E}(q_0)$ is stable. Moreover, according to Theorem I, only the contact normals play a role in the stance's stability. But first let us determine the equilibrium region $\mathcal{E}(q_0)$. According to Proposition 5.1, an equilibrium exists iff the vertical direction e lies in the positive span of the contact normals $\hat{l}_1, \hat{l}_2, \hat{l}_3$. If this condition is satisfied, L can intersect $N(q_0)$ in the following two ways (see Fig. 5(c)). If $\hat{l}_1, \hat{l}_2, \hat{l}_3$ positively span only a portion of the physical plane, L intersects $N(q_0)$ along a finite interval. If $\hat{l}_1, \hat{l}_2, \hat{l}_3$ positively span the entire plane, L intersects $N(q_0)$ along a semi-infinite interval. In the following, p_{ij} denotes the intersection point of the lines l_i and l_j, and l'_{ij} denotes the vertical line through p_{ij}.

First consider the case where $\hat{l}_1, \hat{l}_2, \hat{l}_3$ positively span only a portion of the physical plane. In this case, $\mathcal{E}(q_0)$ is a *vertical strip* with the following two boundaries. If $e = \hat{l}_i$, l_i is one of the two boundaries. If e lies in the interior of the positive span of $\hat{l}_i$ and $\hat{l}_j$, the vertical line l'_{ij} is one of the two boundaries (this could be true for one, two, or none of the pairs of contact normals). The equilibrium region is depicted in Fig. 8(a), where the boundaries of the vertical strip are the lines l'_{12} and l'_{13}. One exceptional case occurs when $e = \hat{l}_i$, such that e is not in the positive span of the other two contact normals. In this case, two supports are nonactive, and $\mathcal{E}(q_0)$ is the vertical line l_i. Next consider the case where $\hat{l}_1, \hat{l}_2, \hat{l}_3$ positively span the entire plane. In this case, e must lie either in the same direction as exactly one of the contact normals, or in the interior of the positive span of exactly one pair of contact normals $\hat{l}_i$ and $\hat{l}_j$. If e lies in the same direction as $\hat{l}_i$, $\mathcal{E}(q_0)$ is the *vertical half-plane* bounded by l_i that does not contain the point p_{jk} where the other two lines intersect. If e lies in the interior of the positive span of $\hat{l}_i$ and $\hat{l}_j$, $\mathcal{E}(q_0)$ is the *vertical half-plane* bounded by l'_{ij}, lying on the side of l'_{ij} that does not contain the points p_{ik} and p_{jk}. Fig. 8(b) depicts the vertical half-plane for the case where e lies in the interior of the positive span of $\hat{l}_1$ and $\hat{l}_2$.

Consider now the stability region $\mathcal{E}^S(q_0)$ for three-contact stances. According to Theorem I, if the c-obstacle normals η_1, η_2, η_3 are linearly independent, stability only requires that $\nabla U(q_0)$ lie in the interior of the normal cone $N(q_0)$. It can be verified that η_1, η_2, η_3 are linearly independent whenever the three lines l_1, l_2, l_3 do not intersect at a single point. In particular, for linear independence, it is required that the lines l_1, l_2, l_3 will not all be parallel to each other (as this corresponds to concurrency at infinity), nor can any two of the lines coincide. In all other cases, η_1, η_2, η_3 are linearly independent and the theorem applies. The condition that $\nabla U(q_0)$ lie in the interior of $N(q_0)$ is satisfied whenever the equilibrium coefficients $\lambda_1, \lambda_2, \lambda_3$ are all positive, i.e., when all the supports are active. Recall that L intersects $N(q_0)$ along a finite or a semi-infinite interval. Then, some of the λ_i's are zero precisely when ∇U lies at an end point of the intersection interval of L with $N(q_0)$. The values of $x_{\rm cm}$ corresponding to these end points occur at the vertical lines that bound the equilibrium region. Thus, for three-contact stances, $\mathcal{E}^S(q_0)$ always *includes the interior* of the equilibrium region $\mathcal{E}(q_0)$.

Finally consider stances involving $k \geq 4$ contacts. For such stances, $\mathcal{E}(q_0)$ is a union of the individual equilibrium regions resulting from every subset of three contacts. Note that this union is always a convex connected region in the plane. Hence, for $k \geq 4$ contacts, $\mathcal{E}(q_0)$ is a single vertical strip, a single half-plane, or else the entire plane. The stratum containing q_0 is generically zero-dimensional in these cases, so for $k \geq 4$ contacts, the stability region $\mathcal{E}^S(q_0)$ always contains the interior of the equilibrium region $\mathcal{E}(q_0)$.

VI. Quasi-static Locomotion Synthesis

This section sketches a quasi-static locomotion paradigm for a three-legged robot moving on a piecewise linear terrain in 2-D. We synthesize a 3–2–3 gait pattern consisting of three-legged stances interleaved by two-legged stances. During three-legged stances, the robot repositions its center-of-mass; during two-legged stances, it places a leg at a new position. In order to guarantee stability of the mechanism, its center-of-mass must move within the stability strip associated with three-legged stances, and within the stable lower half-line associated with two-legged stances. However, limb lifting during a two-legged stance shifts the mechanism's center-of-mass and causes sliding of the contacts to a new equilibrium stance. Hence, we identify for each two-legged stance a *bounded sliding region*, where the robot's center-of-mass may move without causing contact sliding beyond an allowed tolerance. Furthermore, some amount of friction is always present at the contacts. We discuss how friction provides robustness with respect to small foot placement errors, as well as yielding better stability properties of the frictionless stances. Simulation of a 3–2–3 maneuver illustrates the locomotion synthesis paradigm.

A. Bounded Sliding of Frictionless Equilibrium Stances

Given a nominal two-contact equilibrium stance, we first compute the change in $\mathcal{B}$'s equilibrium configuration due to a small change in its center-of-mass position. Then we identify a neighborhood of configurations that lies in the basin of attraction of the *new* equilibrium. The latter set is used next to guarantee bounded contact sliding during limb lifting. Let $\Delta \boldsymbol{r}_{\rm cm} = (\Delta x_{\rm cm}, \Delta y_{\rm cm})$ denote the shift in $\mathcal{B}$'s center-of-mass expressed in $\mathcal{B}$'s body frame, and let $\Delta q_0 = (\Delta d_0, \Delta \theta_0)$ denote the corresponding change in $\mathcal{B}$'s equilibrium configuration. The following lemma gives a first-order approximation for Δq_0 as

a function of $\Delta \boldsymbol{r}_{\rm cm}$, for the case where $\mathcal{B}$ is supported by a piecewise linear terrain.

Lemma 6.1: Let $\mathcal{B}$ be supported at an equilibrium configuration q_0 by two nonhorizontal frictionless linear segments, such that $\mathcal{B}$'s center-of-mass is at $\boldsymbol{r}^0_{\rm cm}$. Then the equilibrium $q_0 + \Delta q_0$ induced by a small center-of-mass shift $\Delta \boldsymbol{r}_{\rm cm}$ still involves two supporting contacts, and $\Delta q_0 = (\Delta d_0, \Delta \theta_0)$ is given to a first-order approximation by

$$\Delta\theta_0 = \frac{\Delta x_{\rm cm}}{y^0_{\rm cm} + \Delta y_{\rm cm} + \kappa(q_0)} \tag{25}$$

and

$$\Delta d_0 = -\frac{1}{2}([\hat{l}_1\ \hat{l}_2]^T)^{-1} \begin{pmatrix} \kappa_1(q_0) \\ \kappa_2(q_0) \end{pmatrix} (\Delta\theta_0)^2$$

where $mg=1$, $\boldsymbol{r}^0_{\rm cm}=(x^0_{\rm cm}, y^0_{\rm cm})$, $\Delta \boldsymbol{r}_{\rm cm} = (\Delta x_{\rm cm}, \Delta y_{\rm cm})$; $\kappa(q_0)=\lambda_1\kappa_1(q_0)+\lambda_2\kappa_2(q_0)$ such that $\kappa_i(q_0) = \rho_i - r_{\mathcal{B}_i}$ for $i = 1, 2$; and $\hat{l}_1, \hat{l}_2$ are the contact normals at q_0.

A proof of the lemma appears in Appendix II. Some insight into the formula for $\Delta\theta_0$ is as follows. First consider the denominator. The gravity relative curvature form at q_0 is $\kappa_G(q_0, \dot{q}) = y^0_{\rm cm} + \kappa(q_0)$ (where $\dot{q}$ is a unit-magnitude instantaneous rotation of $\mathcal{B}$ about the intersection point of the contact normals). The stable region for $\mathcal{B}$'s center-of-mass is a lower half-line determined by the condition $\kappa_G(q_0, \dot{q}) < 0$. If $\boldsymbol{r}^0_{\rm cm}$ lies in the interior of the stable half-line, for a small $\Delta \boldsymbol{r}_{\rm cm}$, the new equilibrium is still stable and satisfies $y^0_{\rm cm} + \Delta y_{\rm cm} + \kappa(q_0) < 0$. At the numerator, $-\Delta x_{\rm cm}$ is the torque generated by $\Delta \boldsymbol{r}_{\rm cm}$. Thus, (25) gives an equilibrium at $\theta_0 + \Delta\theta_0$ such that $\Delta\theta_0$ has the same sign as the torque generated by $\Delta \boldsymbol{r}_{\rm cm}$. Conversely, when $\boldsymbol{r}^0_{\rm cm}$ lies in the unstable upper half-line, the torque generated by $\Delta \boldsymbol{r}_{\rm cm}$ is destabilizing, and (25) gives an equilibrium at $\theta_0 + \Delta\theta_0$ such that $\Delta\theta_0$ has the opposite sign of the torque generated by $\Delta \boldsymbol{r}_{\rm cm}$.

Let $\theta_{\max}$ be a given tolerance for $\mathcal{B}$'s allowed rotation during a shift of its center-of-mass from $\boldsymbol{r}^0_{\rm cm}$ to $\boldsymbol{r}^0_{\rm cm} + \Delta \boldsymbol{r}_{\rm cm}$. We wish to determine the constraint on $\Delta \boldsymbol{r}_{\rm cm}$ so that $\mathcal{B}$'s motion to the equilibrium associated with $\boldsymbol{r}^0_{\rm cm} + \Delta \boldsymbol{r}_{\rm cm}$ would respect the $\theta_{\max}$ tolerance. Let $\tilde{U}$ denote the gravitational potential of $\mathcal{B}$ when its center-of-mass is at $\boldsymbol{r}^0_{\rm cm} + \Delta \boldsymbol{r}_{\rm cm}$. The local minimum of $\tilde{U}$ at the new equilibrium determines a region of allowed center-of-mass shifts as follows.

Lemma 6.2 Let $q_0 = (d_0, \theta_0)$ be a stable two-contact equilibrium stance associated with $\mathcal{B}$'s center-of-mass at $\boldsymbol{r}^0_{\rm cm}$. Let $\theta_{\max} > 0$ be an upper bound on the allowed change of $\mathcal{B}$'s orientation with respect to θ_0. Then the region of center-of-mass shifts guaranteeing that $\mathcal{B}$'s orientation remains in $[-\theta_{\max}, \theta_{\max}]$ is the downward pointing cone given by

$$\mathcal{A}(\theta_{\max}) = \left\{ \Delta \boldsymbol{r}_{\rm cm} = \begin{pmatrix} \Delta x_{\rm cm} \\ \Delta y_{\rm cm} \end{pmatrix} : \right.$$
$$\left. |\Delta x_{\rm cm}| \le \frac{1}{2}\theta_{\max} |\kappa(q_0) + y^0_{\rm cm} + \Delta y_{\rm cm}| \right\}$$

where $\boldsymbol{r}^0_{\rm cm} = (x^0_{\rm cm}, y^0_{\rm cm})$.

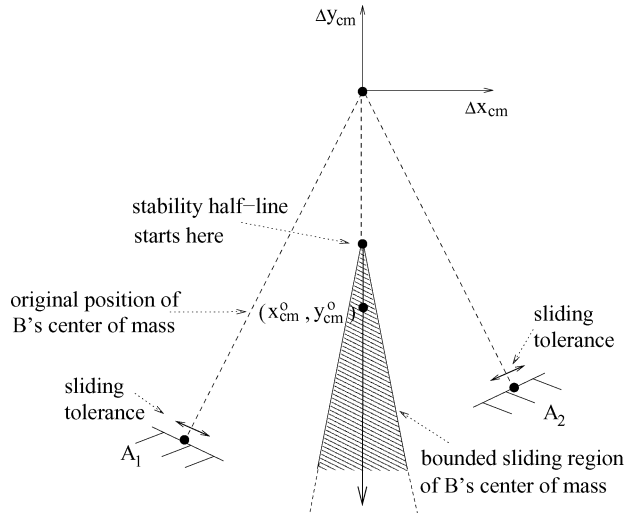

Fig. 9. Bounded sliding region associated with a given $\theta_{\max}$.

The region $\mathcal{A}(\theta_{\max})$ is depicted in Fig. 9. It can be seen that $\mathcal{A}(\theta_{\max})$ has its vertex at the point where the stable lower half-line begins, while its angle is proportional to $\theta_{\max}$.

Proof: Let the double-contact stratum $\mathcal{S}_{12}$ be parametrized by θ. Let $\tilde{U}(\theta)$ be the restriction of $\tilde{U}$ (defined before) to $\mathcal{S}_{12}$. Stability of the equilibrium at $q_0 + \Delta q_0$ implies that $\tilde{U}(\theta)$ has a local minimum at $\theta_0 + \Delta\theta_0$. The quadratic approximation for $\tilde{U}(\theta)$ about $\theta_0 + \Delta\theta_0$ is $\tilde{U}(\theta) = \tilde{U}(\theta_0 + \Delta\theta_0) + 1/2\tilde{U}''(\theta_0 + \Delta\theta_0)(\theta - (\theta_0 + \Delta\theta_0)))^2 + o((\theta - (\theta_0 + \Delta\theta_0))^3)$ such that $\tilde{U}''(\theta_0 + \Delta\theta_0) > 0$. By construction, $\mathcal{B}$ is initially at a zero-velocity orientation θ_0, with its center-of-mass at $\boldsymbol{r}^0_{\rm cm} + \Delta \boldsymbol{r}_{\rm cm}$. Hence, $\mathcal{B}$'s initial total mechanical energy is $\tilde{U}(\theta_0)$. By conservation of energy, $\mathcal{B}$'s dynamic trajectory lies in the set $\{\theta : \tilde{U}(\theta) \le \tilde{U}(\theta_0)\}$ for $t \ge 0$. Focusing on the quadratic approximation of $\tilde{U}$, the latter set is given by $\{\theta : (\theta - (\theta_0 + \Delta\theta_0))^2 \le (\Delta\theta_0)^2\} = \{\theta : |\theta - (\theta_0 + \Delta\theta_0)| \Delta\theta_0\}$. This set is precisely the interval $[\theta_0, \theta_0 + 2\Delta\theta_0]$. Since this interval must lie within $[-\theta_{\max}, \theta_{\max}]$, we obtain the inequality $2|\Delta\theta_0| \le \theta_{\max}$. Substituting for $\Delta\theta_0$ according to (25) gives $|\Delta x_{\rm cm}|/|y^0_{\rm cm} + \Delta y_{\rm cm} + \kappa(q_0)| \le 1/2\theta_{\max}$, which is the formula for $\mathcal{A}(\theta_{\max})$.

To summarize, when a nominal two-contact stance is allowed a sliding tolerance $\theta_{\max}$, the mechanism may quasi-statically move its center-of-mass anywhere within the region $\mathcal{A}(\theta_{\max})$ without incurring contact sliding beyond $\theta_{\max}$. Locomotion planning is thus reduced to the geometric problem of properly chaining the stability strips associated with three-legged stances with the bounded-sliding cones associated with two-legged stances. This is illustrated later, after we discuss the role of friction.

B. Robustness and Stability of Frictional Stances

A bounded-sliding locomotion plan can benefit from friction in two significant ways. First, friction enlarges the two-contact equilibrium line to a vertical strip, thus providing robustness with respect to small foot placement errors. Second, friction provides damping that brings any bounded sliding event to a halt.

First consider the enlarged equilibrium region. The *frictional equilibrium region* of a frictional stance q_0, denoted as $\mathcal{R}(q_0)$, is the set of $\mathcal{B}$'s center-of-mass locations at which the contacts can feasibly maintain a frictional equilibrium against gravity. To characterize $\mathcal{R}(q_0)$, let f_i^n and f_i^t denote the normal and tangential components of the ith contact force f_i. Then the Coulomb friction cone at x_i is given by $\mathcal{C}_i = \{f_i : |f_i^t| \leq \mu f_i^n,\ f_i^n \geq 0\}$, where μ is the coefficient of friction. Let $\mathcal{C}_i^-$ denote the negative reflection of $\mathcal{C}_i$ about x_i. For a given two-contact stance, let Π^{++} denote the infinite vertical strip spanned by the polygon $\mathcal{C}_1 \cap \mathcal{C}_2$. Similarly, let $\Pi^{+-}, \Pi^{-+}, \Pi^{--}$ denote the infinite vertical strips spanned by the polygons $\mathcal{C}_1 \cap \mathcal{C}_2^-, \mathcal{C}_1^- \cap \mathcal{C}_2, \mathcal{C}_1^- \cap \mathcal{C}_2^-$. Note that some of these polygons and their associated strips may be empty. Finally, let Π denote the infinite vertical strip bounded by the contacts x_1 and x_2. The following proposition characterizes the region $\mathcal{R}(q_0)$.

Proposition 6.3: ([30]) Let $\mathcal{B}$ be at a two-contact frictional equilibrium stance configuration q_0 in a 2-D gravitational environment. Then the frictional equilibrium region $\mathcal{R}(q_0)$ is the infinite vertical strip given by

$$\mathcal{R}(q_0) = ((\Pi^{++} \cup \Pi^{--}) \cap \Pi) \cup ((\Pi^{+-} \cup \Pi^{-+}) \cap \overline{\Pi})$$

where $\overline{\Pi}$ is the complement of Π in $I\!R^2$.

For $k > 2$ contacts, $\mathcal{R}(q_0)$ is an infinite vertical strip obtained by taking the convex hull of the pairwise frictional equilibrium strips.

Friction effectively enlarges the two-contact equilibrium line to a vertical strip. As a result, small foot placement errors about a nominal frictionless two-contact stance would still give an equilibrium stance. Next consider the enhanced stability of frictionless equilibrium stances when friction is present at the contacts. The following definition is given for a general planar mechanism $\mathcal{L}$ having a configuration variable x.

Definition 2: [Frictional Stabilty] Let a planar mechanism $\mathcal{L}$ be at an equilibrium configuration x_0 that involves contact with several stationary bodies. Let $\mathcal{X}$ be the stratified set of $\mathcal{L}$'s free configurations. Then, $\mathcal{L}$ has *frictional stability* at x_0 if, for any neighborhood $\mathcal{V}$ of x_0, there exists a neighborhood $\mathcal{W} \subseteq \mathcal{V}$ containing x_0 such that all trajectories that start in $\mathcal{W}$ with sufficiently small velocity stay inside $\mathcal{V}$ for $t \geq 0$, and eventually converge to some zero-velocity equilibrium configuration in $\mathcal{V}$.

Frictional stability implies the usual stability of the zero-velocity state $(x_0, 0)$. However, it does not require convergence to the original equilibrium, but rather to some nearby equilibrium. It is the best stability one can hope for in the context of quasi-static locomotion, where the object representing the mechanism is supported by *passive* frictional contacts against gravity. When $\mathcal{L}$ is influenced by a potential energy U and x_0 is a strict local minimum U, the level sets of U form bounded neighborhoods about x_0. In this case, $\mathcal{L}$ possesses frictional stability at x_0 if its trajectories are damped by contact friction and suitable control laws at the mechanism's joints. The following theorem asserts this fact for the case of a rigid object $\mathcal{B}$ in a 2-D gravitational environment.

Therom 2: Let a planar object $\mathcal{B}$ be at an equilibrium stance configuration q_0 in a gravitational environment, with friction present at the contacts. If q_0 is a nondegenerate local minimum of the gravitational potential energy U in $\mathcal{F}$, $\mathcal{B}$ possesses *frictional stability* at q_0.

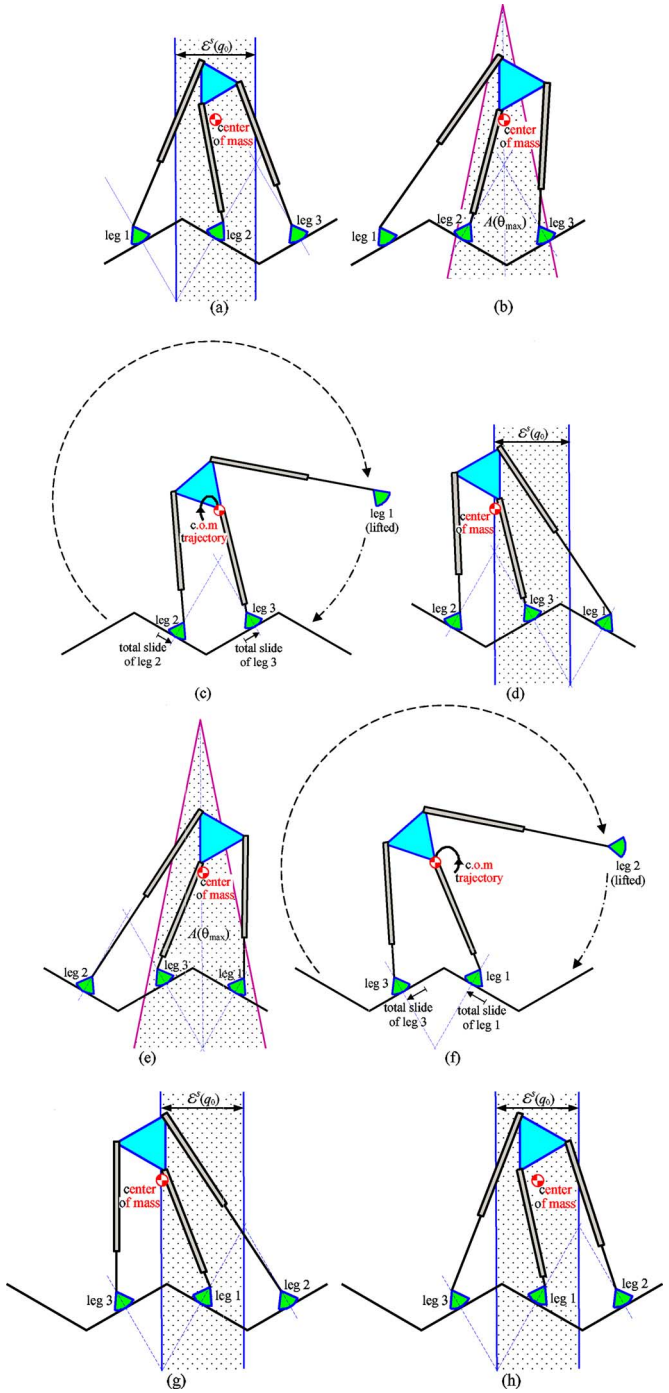

Fig. 10. 3–2–3 quasi-static locomotion maneuver. (a) and (b) Initial three-legged phase. (c) Bounded sliding two-legged phase. (d) and (e) Three-legged phase. (f) Bounded sliding two-legged phase. (g) and (h) Final three-legged phase.

A proof of the theorem is relegated to [37]. Frictional stability of a nominal equilibrium stance ensures that when $\mathcal{B}$ is perturbed, it will converge to some frictional equilibrium stance in the vicinity of the original stance. This effect of friction guarantees that any bounded sliding event under our locomotion plan would halt at some nearby frictional equilibrium stance.

C. Synthesis of 3–2–3 Locomotion Maneuver

A 3–2–3 locomotion maneuver is illustrated with a three-legged mechanism moving on a piecewise linear terrain, as shown in Fig. 10. The terrain consists of uniform 1-m-long segments having $\pm 30^\circ$ slopes. The robot consists of three legs attached to a central base via rotational joints (the legs' specific kinematic structure is ignored). The central base weighs 10 kg, each footpad weighs 1 kg, and the legs themselves are assumed to have negligible mass. Each footpad is bounded by a circular curve having a radius of 2.5 m.

The maneuver begins with the three-legged stance shown in Fig. 10(a). The robot decides that leg 1 should be lifted to a new position. In preparation for this limb lifting, the robot moves its center-of-mass within the stability strip $\mathcal{E}^S(q_0)$ while keeping its footholds fixed. This stage ends when the robot's center-of-mass reaches the equilibrium line associated with legs 2 and 3, shown in Fig. 10(b). The figure also shows the lower cone $\mathcal{A}(\theta_{\max})$ associated with a sliding tolerance of 0.2 m. Before lifting leg 1, the robot selects a new foothold for this leg such that the mechanism's center-of-mass would remain inside $\mathcal{A}(\theta_{\max})$ during limb lifting. The path taken by the mechanism's center-of-mass during the lifting of leg 1, together with the net sliding incurred at the contact, are shown in Fig. 10(c). The stability strip associated with the new three-legged stance is shown in Fig. 10(d). From now on, the process repeats itself. The robot next lifts leg 2. It moves its center-of-mass to the equilibrium line of legs 1 and 3 as shown in Fig. 10(e). This figure also shows the lower cone $\mathcal{A}(\theta_{\max})$ associated with a 0.2 m sliding tolerance. The robot now lifts and places leg 2 at a new position, as shown in Fig. 10(f) and (g). Finally, the robot moves its center-of-mass forward, thus completing a full cycle relative to the supporting terrain (see {http://robots.technion.ac.il/spider.htm} for an animation of this maneuver).

It should be emphasized that the example illustrates the quasi-static motion scheme, but otherwise lacks several important components. Most importantly, the mechanism's dynamics should be included, showing the actual bounded-sliding trajectory taken by the robot under the influence of frictional contacts. However, note that friction would only enhance the locomotion scheme, giving foot-placement robustness and convergence of any bounded sliding event to a nearby frictional equilibrium stance.

VII. Conclusion

The paper derived a generic stance stability test for an object $\mathcal{B}$ supported by k frictionless contacts against a potential field such as gravity. The stability test contains a first-derivative part that accounts for contact breaking motions, and a second-derivative part that accounts for motions that maintain simultaneous contact with the k supporting bodies. When the stability test is expressed in terms of the bodies' geometry, stance stability depends on surface normals as well as surface curvature for $k=1,2$ contacts in 2-D and $k=1\ldots5$ contacts in 3-D. Stance stability depends only on surface normals for a higher number of contacts. The stability test was subsequently applied to a planar object $\mathcal{B}$ supported by a fixed set of contacts and having a variable center-of-mass. We identified the stable equilibrium region $\mathcal{E}^S(q_0)$ for the various k-contact stances in 2-D. Based on these regions, we sketched a quasi-static locomotion plan for a three-legged mechanism over a piecewise linear terrain. During limb lifting, the procedure maintains the robot's center-of-mass within a downward pointing cone guaranteeing a user-specified sliding tolerance. Finally, friction was shown to provide robustness with respect to small foot placement errors as well as better stability of the frictionless locomotion plan. To our knowledge, this quasi-static locomotion scheme is currently the only one that takes curvature effects into account.

Consider now implications of the stance stability test to 3-D terrains [20]. For $k=1,2$ contacts, $\mathcal{E}^S(q_0)$ is generically empty unless the terrain is a horizontal plane. For $k=3,4$ contacts $\mathcal{E}^S(q_0)$ is generically a vertical *lower half-line*, while for $k=5$ contacts it is generically a vertical *lower half-strip*. For $k\geq 6$ contacts, $\mathcal{E}^S(q_0)$ is generically a vertical *3-D prism* with a polygonal cross section. However, the latter prism matches the one generated by the classical support polygon only on horizontal flat terrains. On typical uneven terrains, the stable prism is only *a subset* of the one generated by the support polygon. A paper under preparation will provide a detailed description of these regions, together with a quasi-static locomotion scheme over 3-D terrains.

Finally consider the stability of an object $\mathcal{B}$ supported by frictional contacts. In the frictionless case, the stable equilibria of $\mathcal{B}$ are local minima of its gravitational potential energy. However, no such simple criterion exists for frictional stances. First, one must ensure that a feasible equilibrium stance is actually an equilibrium of the underlying dynamical system. For frictionless equilibrium stances, such a result is automatic [21], [32]. Unfortunately, when friction is present at the contacts, rigid body dynamics can be ambiguous [16], [19]. One promising approach is the *strong equilibrium* criterion [31]. A stance is in strong equilibrium when among all possible static/roll/slip/break reactions at the contacts, static equilibrium is the only dynamically feasible reaction. Second, one must ensure that a candidate equilibrium stance is dynamically stable, based on convergence under small position-and-velocity perturbations. Here too one encounters a complication: the mechanics of friction dictates convergence to some nearby zero-velocity stance rather than to the original stance. The notion of *frictional stability* introduced in this paper captures this behavior. However, while stances selected at local minima of the potential energy function possess frictional stability, it is currently unclear which frictional stances posses this type of stability. All of these open problems need to be resolved in order to achieve safe and reliable quasi-static locomotion planners on general terrains.

Appendix I

SMT Proof Details

This appendix contains proofs of statements made in Sections III and Sections IV. The first proposition gives the SMT condition for a local minimum.

Proposition 3.1 Let f be a Morse function on a regularly stratified set $\mathcal{X}\subset I\!R^m$, and let $x_0\in\mathcal{X}$ be a critical point of f.

Then f has a local minimum at x_0 iff it satisfies the following two conditions

$$l^- = \emptyset \qquad \text{and} \qquad \sigma = 0$$

where σ is the Morse index of f at x_0 and l^- is the lower half link of f at x_0.

Proof: First assume that x_0 is a local minimum of f, with $c_0 = f(x_0)$. In that case, the level set $\mathcal{X}|_{c_0-\epsilon} = \{x \in \mathcal{X} : f(x) = c_0 - \epsilon\}$ must be empty in a sufficiently small neighborhood of x_0, where $\epsilon > 0$ is a small parameter. The lower half link l^- is a subset of this level set; hence, l^- must be empty. As for σ, f has in particular a local minimum along the stratum containing x_0. Hence, $\sigma = 0$.

Assume now that $l^- = \emptyset$ and $\sigma = 0$. According to [8, Theorem 3.12], the topological change in the level sets $\mathcal{X}|_c$ at a critical point x_0 consists of taking a "handle set,"

$$H = D^\sigma \times \mathsf{cone}(l^-)$$

and gluing it to the level set $\mathcal{X}|_{c_0-\epsilon}$ along the "gluing seam,"

$$G = \mathsf{bdy}(D^\sigma) \times \mathsf{cone}(l^-) \cup D^\sigma \times l^-.$$

Several terms in these formulas require explanation. First, D^i denotes the i-dimensional disc and $\mathsf{bdy}(D^i)$ denotes its boundary, the $(i-1)$-dimensional sphere. By definition, D^0 is a single point and $\mathsf{bdy}(D^0)$ is empty. Next, $\mathsf{cone}(l^-)$ is the cone with base set l^- and vertex x_0, i.e., it is the collection of rays emanating from x_0 and passing through the points of l^-. By definition $\mathsf{cone}(l^-) = \{x_0\}$ when l^- is empty.

In our case, $\sigma = 0$ and $l^- = \emptyset$. Hence, the handle set is $H = D^0 \times \{x_0\}$, which is topologically equivalent to the single-point set $H = \{x_0\}$. Furthermore, the gluing seam G is empty, since both $\mathsf{bdy}(D^0)$ and l^- are empty. Since G is empty, the handle set H is disjoint from the sublevel set $\mathcal{X}|_{\leq c_0-\epsilon} = \{x \in \mathcal{X} : f(x) \leq c_0 - \epsilon\}$ in a local neighborhood centered at x_0. Since H and $\mathcal{X}|_{\leq c_0-\epsilon}$ are additionally closed sets, a sufficiently small neighborhood about $H = \{x_0\}$ contains no points from the sublevel set $\mathcal{X}|_{\leq c_0-\epsilon}$. Hence, x_0 is a local minimum of f in $\mathcal{X}$.

The next lemma gives a geometric test for $l^- = \emptyset$. The lemma uses the notion of polar cones. Let C_1 and C_2 be two cones in $\mathbb{R}^m$, both having their vertex at the origin. Then C_1 is *polar* to C_2 if every vector $v \in C_1$ satisfies $w \cdot v \leq 0$ for all vectors $w \in C_2$.

Lemma 4.1: Let $f : \mathcal{F} \to \mathbb{R}$ be a smooth function. Let q_0 be a critical point of f on a stratum $\mathcal{S}$ of $\mathcal{F}$, such that $\mathcal{S}$ is the intersection of k c-obstacle boundaries, $\mathcal{S} = \cap_{i=1}^k \mathcal{S}_i$. A necessary condition for the lower half link at q_0, l^-, to be *empty* is:

$$\nabla \tilde{f}(q_0) = \sum_{i=1}^{k} \lambda_i \eta_i(q_0), \tag{26}$$

for some scalars $\lambda_1, \ldots, \lambda_k$ such that $\lambda_i \geq 0$ for $i = 1, \ldots, k$. Moreover, if the λ_i's are all strictly positive, (3) is also sufficient for $l^- = \emptyset$.

Proof: First we prove that $l^- = \emptyset$ implies (26). The lower half link is given by $l^- = E(q_0) \cap f^{-1}(c_0 - \epsilon)$, where $E(q_0)$ is the normal slice at q_0 and $c_0 = f(q_0)$. Let $\mathsf{span}(\eta_1 \ldots \eta_k)$ denote the subspace based at q_0 and spanned by the c-obstacle normals $\eta_1(q_0), \ldots, \eta_k(q_0)$. We may assume that $E(q_0)$ is the intersection of a small disc in $\mathsf{span}(\eta_1, \ldots, \eta_k)$ with $\mathcal{F}$. If l^- is empty, f must be nondecreasing along any c-space path that starts at q_0 and stays in $E(q_0)$. Let $C(q_0)$ denote the collection of tangent vectors that are based at q_0 and point into $E(q_0)$. This collection can be characterized as follows. Recall that the tangent cone at q_0 is $M(q_0) = \{\dot{q} : \eta_i(q_0) \cdot \dot{q} \geq 0 \text{ for } i = 1, \ldots, k\}$. Then $C(q_0) = M(q_0) \cap \mathsf{span}(\eta_1 \ldots \eta_k)$, which is a subcone of $M(q_0)$.

Let $q(t)$ be a c-space path that starts at $q(0) = q_0$ and lies in $E(q_0)$. Then its tangent $\dot{q}(0) = \dot{q}$ lies in $C(q_0)$. Since l^- is empty, $d/dt|_{t=0} f(q(t)) = \nabla \tilde{f}(q_0) \cdot \dot{q} \geq 0$ for *all* $\dot{q} \in C(q_0)$. But this condition is equivalent to the requirement that $\nabla \tilde{f}(q_0)$ be in the cone polar to the negated cone $-C(q_0)$. Our goal now is to characterize the cone polar to $-C(q_0)$. Consider the normal cone at q_0, $N(q_0) = \{\sum_{i=1}^k \lambda_i \eta_i(q_0) : \lambda_i \geq 0 \text{ for } i = 1, \ldots, k\}$. Let $-N(q_0)$ be the negated normal cone. Then a key property is that *the tangent cone $M(q_0)$ is polar to the negated normal cone $-N(q_0)$*. Since $C(q_0)$ is a subcone of $M(q_0)$, $C(q_0)$ is also polar to $-N(q_0)$. Hence, the cone polar to $-C(q_0)$ is precisely the normal cone $N(q_0)$, and $\nabla \tilde{f}(q_0) \in N(q_0)$ as stated in (26).

Next, we prove that (26) implies $l^- = \emptyset$ when λ_i's are strictly positive. First observe that any nonzero tangent vector $\dot{q} \in \mathsf{span}(\eta_1, \ldots, \eta_k)$ satisfies $\eta_i \cdot \dot{q} \neq 0$ for some $1 \leq i \leq k$. On the other hand, any tangent vector $\dot{q} \in C(q_0)$ lies in the tangent cone $M(q_0)$, where $\eta_i(q_0) \cdot \dot{q} \geq 0$ for $i = 1, \ldots, k$. Thus, $\eta_i(q_0) \cdot \dot{q} > 0$ for some i. Since $d/dt|_{t=0} f(q(t)) = \nabla \tilde{f}(q_0) \cdot \dot{q} = \sum_{i=1}^k \lambda_i (\eta_i(q_0) \cdot \dot{q})$ according to (26), it must be that $d/dt|_{t=0} f(q(t)) > 0$. Thus, f strictly increases along all c-space paths that start at q_0 and lie in $E(q_0)$. Hence, $l^- = \emptyset$.

The last lemma specifies under what conditions U is a Morse function.

Lemma 4.3 it Let $q_0 \in \mathcal{S}$ be an equilibrium configuration of $\mathcal{B}$, where $\mathcal{S} = \cap_{i=1}^k \mathcal{S}_i$. Then U is *Morse* at q_0 if first $\nabla U(q_0)$ lies in the interior of the normal cone $N(q_0)$, and second, if the eigenvalues of the matrix of $\kappa_U(q_0, \dot{q})$, which is $\sum_{i=1}^k \lambda_i D\eta_i(q_0) - D^2U(q_0)$, are nonzero.

Proof: First we show that, if $\nabla U(q_0)$ lies in the interior of the normal cone $N(q_0)$, it cannot be normal to any neighboring stratum. Let $\mathcal{T}$ be a neighbor stratum of $\mathcal{S}$ in $\mathcal{F}$. Let $q(t)$ be a path in $\mathcal{T}$ that approaches $q_0 \in \mathcal{S}$. As $q(t)$ approaches q_0, the normal cone to $\mathcal{T}$ along $q(t)$ has a limit. This limit is a cone spanned by a subcollection of the c-obstacle normals $\eta_1(q_0), \ldots, \eta_k(q_0)$. Let $\eta_{i_1}(q_0), \ldots, \eta_{i_l}(q_0)$ be this sub-collection, where $1 \leq l < k$. For $k \leq m$ contacts with linearly independent contact normals, the positive combination of $\eta_{i_1}(q_0), \ldots, \eta_{i_l}(q_0)$ automatically lies on the boundary of the normal cone $N(q_0)$. Moreover, it can be verified that any vector normal to $\mathcal{T}$ at q_0 lies in the subspace spanned by $\eta_{i_1}(q_0), \ldots, \eta_{i_l}(q_0)$. Hence, for $k \leq m$ contacts, if $\nabla U(q_0)$ lies in the interior of $N(q_0)$, it cannot possibly be normal to the stratum $\mathcal{T}$.

For $k > m$ contacts, such that the $m \times k$ matrix $[\eta_1 \cdots \eta_k]$ has full rank, the interior of the normal cone $N(q_0)$ is an open subset of the ambient space $\mathbb{R}^m$. If $\nabla U(q_0)$ lies in the interior of $N(q_0)$, any vector $\nabla U(q_0) - \epsilon v$ also lies in $N(q_0)$, where $v \in \mathbb{R}^m$ and

$\epsilon > 0$ is sufficiently small. Consider now a path $q(t)$ that starts at q_0 and lies in the stratum $\mathcal{T}$. Since $q(t)$ lies in the freespace, its tangent vector $\dot{q} = \dot{q}(0)$ satisfies $\eta_i(q_0) \cdot \dot{q} \geq 0$ for $i = 1, \ldots, k$. The vector $n = \nabla U(q_0) - \epsilon\dot{q}$ belongs to $N(q_0)$ for a sufficiently small ϵ. Hence, n is positively spanned by $\eta_1(q_0), \ldots, \eta_k(q_0)$, i.e., $n = \lambda_1\eta_1(q_0) + \cdots + \lambda_k\eta_k(q_0)$ for some $\lambda_i \geq 0$. Since $\eta_i(q_0) \cdot \dot{q} \geq 0$ for $i = 1, \ldots, k$, the vector $n \in N(q_0)$ satisfies $n \cdot \dot{q} \geq 0$. However, if $\nabla U(q_0)$ is normal to the stratum $\mathcal{T}$, $\nabla U(q_0) \cdot \dot{q} = 0$, and in this case, $n \cdot \dot{q} = (\nabla U(q_0) - \epsilon\dot{q}) \cdot \dot{q} = -\epsilon\dot{q}^2 < 0$. Thus, if $\nabla U(q_0)$ lies in the interior of $N(q_0)$, it cannot be normal to the stratum $\mathcal{T}$.

As for the other condition, we have shown in the proof of Proposition 4.2 that $\ddot{U}(q_0) = -\kappa_U(q_0, \dot{q})$ along trajectories $q(t)$ in $\mathcal{S}$. This shows that the restriction of $D^2U(q_0)$ to $T_{q_0}\mathcal{S}$ is equal to the negated matrix of $\kappa_U(q_0, \dot{q})$. Hence, if the eigenvalues of the matrix of $\kappa_U(q_0, \dot{q})$ are nonzero, so must be the eigenvalues of $D^2U(q_0)$.

APPENDIX II
LOCOMOTION SYNTHESIS PROOF DETAILS

This appendix contains a proof of the formula for the change in $\mathcal{B}$'s equilibrium configuration due to a small shift in its center-of-mass. The ensuing analysis assumes that, at the nominal stance, $\mathcal{B}$'s body frame lies along the vertical line passing through the intersection point of the contact normals, so that $\boldsymbol{r}^0_{\rm cm}$ is collinear with the vertical direction $\boldsymbol{e}$.

Lemma 6.1: Let $\mathcal{B}$ be supported at an equilibrium configuration q_0 by two nonhorizontal frictionless linear segments, such that $\mathcal{B}$s center-of-mass is at $\boldsymbol{r}^0_{\rm cm}$. Then the equilibrium $q_0 + \Delta q_0$ induced by a small center-of-mass shift $\Delta\boldsymbol{r}_{\rm cm}$ still involves two supporting contacts, and $\Delta q_0 = (\Delta d_0, \Delta\theta_0)$ is given to a first-order approximation by

$$\Delta\theta_0 = \frac{\Delta x_{\rm cm}}{y^0_{\rm cm} + \Delta y_{\rm cm} + \kappa(q_0)} \tag{27}$$

and

$$\Delta d_0 = -\frac{1}{2}([\hat{l}_1\ \hat{l}_2]^T)^{-1}\begin{pmatrix}\kappa_1(q_0)\\ \kappa_2(q_0)\end{pmatrix}(\Delta\theta_0)^2$$

where $mg = 1$, $\boldsymbol{r}^0_{\rm cm} = (x^0_{\rm cm}, y^0_{\rm cm})$, $\Delta\boldsymbol{r}_{\rm cm} = (\Delta x_{\rm cm}, \Delta y_{\rm cm})$; $\kappa(q_0) = \lambda_1\kappa_1(q_0) + \lambda_2\kappa_2(q_0)$ such that $\kappa_i(q_0) = \rho_i - r_{\mathcal{B}_i}$ for $i = 1, 2$; and $\hat{l}_1, \hat{l}_2$ are the contact normals at q_0.

Proof: First we establish that any equilibrium stance in the vicinity of q_0 still involves two contacts. The configuration q_0 lies on $\mathcal{S}_{12}$ that forms the common boundary of the single-contact strata $\mathcal{S}_1$ and $\mathcal{S}_2$. A single-contact equilibrium on $\mathcal{S}_i$ $(i = 1, 2)$ requires that the contact normal $\hat{l}_i$ be collinear with the vertical direction $\boldsymbol{e}$. Since the two supporting segments are nonhorizontal and frictionless, none of these segments can be involved in a single-contact equilibrium stance.

Next we construct a second-order approximation for the c-obstacle boundaries at q_0. Let $\mathsf{dst}_i(q)$ denote the signed distance of a configuration q from $\mathcal{S}_i$, such that dst_i is negative inside the c-obstacle, zero on its boundary, and positive outside the c-obstacle. Thus, $\mathcal{S}_i = \{q \in I\!R^3 : \mathsf{dst}_i(q) = 0\}$ for $i = 1, 2$. It can be verified that dst_i is smooth in the vicinity of q_0 in the usual case where the contacts lie in the interior of the supporting segments. It can be further verified that $\nabla\mathsf{dst}_i(q_0) = \eta_i(q_0)$ and $D^2\mathsf{dst}_i(q_0) = D\eta_i(q_0)$ for $i = 1, 2$. Hence, $\mathsf{dst}_i(q) = \eta_i(q_0) \cdot (q - q_0) + 1/2(q - q_0)^T D\eta_i(q_0)(q - q_0) + o(\mathrm{q} - \mathrm{q_0}^3)$, where we substituted $\mathsf{dst}_i(q_0) = 0$. The second-order approximation of $\mathcal{S}_i$, denoted by $\tilde{\mathcal{S}}_i$, is given by $\tilde{\mathcal{S}}_i = \{q \in I\!R^3 : \eta_i(q_0) \cdot (q - q_0) + 1/2(q - q_0)^T D\eta_i(q_0)(q - q_0) = 0\}$, where $D\eta_i(q_0)$ is the curvature matrix of $\mathcal{S}_i$ at q_0.

We now write the two-contact equilibrium equation (1) in terms of the normals to $\tilde{\mathcal{S}}_1$ and $\tilde{\mathcal{S}}_2$, given by $\tilde{\eta}_i(q) = \eta_i(q_0) + D\eta_i(q_0)(q - q_0)$ for $i = 1, 2$. The equilibrium equation requires unit-magnitude normals, $\tilde{\eta}_1/\tilde{\eta}_1$ and $\tilde{\eta}_2/\tilde{\eta}_2$, which we now compute. Since $\mathcal{B}$'s frame origin is at the intersection point of the contact normals $\eta_i(q_0) = (\hat{l}_i, 0)$ for $i = 1, 2$. When the flat curvature of the supporting contacts is substituted into the c-obstacle curvature formula (14), one obtains the 3×3 curvature matrix:

$$D\eta_i(q_0) = \begin{bmatrix}0 & 0\\ 0 & \kappa_i(q_0)\end{bmatrix}, \qquad \text{for } i = 1, 2 \tag{28}$$

where $\kappa_i(q_0) = \rho_i - r_{\mathcal{B}_i}$ is the curvature of $\mathcal{S}_i$ at q_0 along instantaneous rotation of $\mathcal{B}$ about the contact normals' intersection point. Thus, $\tilde{\eta}_i(q) = \big(\hat{l}_i, \kappa_i(q_0)(\theta - \theta_0)\big)$ and $\tilde{\eta}_i = \sqrt{1 + \kappa_{\rm i}(\mathrm{q_0})^2(\theta - \theta_0)^2} = 1 + o((\theta - \theta_0)^2)$. It follows that $\tilde{\eta}_1 = \tilde{\eta}_2 = 1$ up to a first-order approximation. Using a similar approach, it can be verified that λ_1 and λ_2 in (1) also remain constant to a first-order approximation. Substituting $\Delta\theta_0 = \theta - \theta_0$ in $\tilde{\eta}_1$ and $\tilde{\eta}_2$, and using formula (12) for ∇U, the new equilibrium at $q_0 + \Delta q_0$ satisfies

$$\lambda_1\begin{pmatrix}\hat{l}_1\\ \kappa_1(q_0)\Delta\theta_0\end{pmatrix} + \lambda_2\begin{pmatrix}\hat{l}_2\\ \kappa_2(q_0)\Delta\theta_0\end{pmatrix} = mg\begin{pmatrix}\boldsymbol{e}\\ \rho_{\rm cm}(q_0 + \Delta q_0, \boldsymbol{r}^0_{\rm cm} + \Delta\boldsymbol{r}_{\rm cm}) \times \boldsymbol{e}\end{pmatrix} \tag{29}$$

where $\boldsymbol{\rho}_{\rm cm}(q, \boldsymbol{r}_{\rm cm}) = R(\theta)\boldsymbol{r}_{\rm cm}$. We now derive an expression for $\boldsymbol{\rho}_{\rm cm}(q_0 + \Delta q_0, \boldsymbol{r}^0_{cm} + \Delta\boldsymbol{r}_{\rm cm}) = R(\theta_0 + \Delta\theta_0)(\boldsymbol{r}^0_{\rm cm} + \Delta\boldsymbol{r}_{\rm cm})$. The Taylor expansion of $R(\theta)$ at θ_0 is $R(\theta) = I + (\theta - \theta_0)J + o((\theta - \theta_0)^2)$. Hence, to a first-order approximation, $\boldsymbol{\rho}_{\rm cm}(q_0 + \Delta q_0, \boldsymbol{r}^0_{\rm cm} + \Delta\boldsymbol{r}_{\rm cm}) = (I + \Delta\theta_0 J)(\boldsymbol{r}^0_{\rm cm} + \Delta\boldsymbol{r}_{\rm cm})$. Therefore, $\boldsymbol{\rho}_{\rm cm}(q_0 + \Delta q_0, \boldsymbol{r}^0_{\rm cm} + \Delta\boldsymbol{r}_{\rm cm}) \times \boldsymbol{e} = \Delta\boldsymbol{r}_{\rm cm} \times \boldsymbol{e} + \Delta\theta_0\big(J(\boldsymbol{r}^0_{\rm cm} + \Delta\boldsymbol{r}_{\rm cm})\big) \times \boldsymbol{e} = \Delta x_{\rm cm} - \Delta\theta_0(y^0_{\rm cm} + \Delta y_{\rm cm})$, where we used the fact that $\boldsymbol{r}^0_{\rm cm}$ is collinear with $\boldsymbol{e}$. The torque part of (29) is therefore $\big(\lambda_1\kappa_1(q_0) + \lambda_2\kappa_2(q_0)\big)\Delta\theta_0 = \Delta x_{\rm cm} - \Delta\theta_0(y^0_{\rm cm} + \Delta y_{\rm cm})$, where we substituted $mg = 1$. Solving this equation for $\Delta\theta_0$ gives the left part of (27).

Last consider the solution for Δd_0. The stratum $\mathcal{S}_{12}$ is 1-D and a solution for $\Delta\theta_0$ determines a solution for Δd_0 as follows. The second-order approximation for $\mathcal{S}_{12}$ is given by the intersection $\tilde{\mathcal{S}}_1 \cap \tilde{\mathcal{S}}_2$, where $\tilde{\mathcal{S}}_i = \{q \in I\!R^3 : \hat{l}_i \cdot (d - d_0) + 1/2\kappa_i(q_0)(\theta - \theta_0)^2 = 0\}$ for $i = 1, 2$. Substituting $\Delta d_0 = d - d_0$ and $\Delta\theta_0 = \theta - \theta_0$ in the expressions for $\tilde{\mathcal{S}}_1$ and $\tilde{\mathcal{S}}_2$ gives two linear equations in Δd_0. Solving these equations for Δd_0 gives the right-hand side of (27).

REFERENCES

[1] S. Akella and M. T. Mason, "Using partial sensor information to orient parts," *Int. J. Robot. Res.*, vol. 18, no. 10, pp. 963–997, 1999.

[2] J. D. Bernheisel and K. M. Lynch, "Stable transport of assemblies: Pushing stacked parts," *IEEE Trans. Robot. Autom.*, vol. 22, no. 4, pp. 740–750, Aug. 2006.

[3] A. Bicchi, "On the problem of decomposing grasp and manipulation forces in multiple whole-limb manipulation," *Int. J. Robot. Auton. Syst.*, vol. 13, no. 4, pp. 127–147, 1994.

[4] A. Bicchi, "Hands for dexterous manipulation and robust grasping: A difficult road toward simplicity," *IEEE Trans. Robot. Autom.*, vol. 16, no. 6, pp. 652–662, Dec. 2000.

[5] S. J. Blind, C. C. McCullough, S. Akella, and J. Ponce, "Maipulating parts with an array of pins: A method and a machine," *Int. J. Robot. Res.*, vol. 20, no. 10, pp. 808–818, 2001.

[6] T. Bretl, "Motion planning of multi-limbed robots subject to equilibrium constraints: The free-climbing robot problem," *Int. J. Robot. Res.*, vol. 25, no. 4, pp. 317–342, 2006.

[7] M. A. Erdmann, "An exploration of nonprehensile two-palm manipulation," *Int. J. Robot. Res.*, vol. 17, no. 5, pp. 485–503, 1998.

[8] M. Goresky and R. Macpherson, *Stratified Morse Theory*. New York: Springer-Verlag, 1980.

[9] A. Greenfield, A. Rizzi, and H. Choset, "Dynamic ambiguities in frictional rigid-body systems with application to climbing via bracing," in *Proc. IEEE Int. Conf. Robot. Autom.*, 2005, pp. 1959–1964.

[10] K. Hirai, M. Hirose, Y. Haikawa, and T. Takenaka, "The development of Honda humanoid robot," in *Proc. IEEE Int. Conf. Robot. Autom.*, 1998, pp. 1321–1326.

[11] H. Hirukawa, S. Kajita, F. Kanehiro, K. Kaneko, and T. Isozumi, "The human-size humanoid robot that can walk, lie down and get up," *Int. J. Robot. Res.*, vol. 24, no. 9, pp. 755–769, 2005.

[12] D. E. Koditschek, "The application of total energy as a lyapunov function for mechanical control systems," in *Control Theory and Multibody Systems, AMS Series in Contemporary Mathematics,* vol. 97, J. Marsden, P. Krishnaprasad, and J. Simo, Eds. Cambridge, MA, 1989, pp. 131–158, MIT Press.

[13] D. J. Kriegman, "Capture regions of curved 3D objects," in *Proc. IEEE Int. Conf. Robot. Autom.*, 1994, pp. 595–601.

[14] J. Kuffner, K. Nishiwaki, S. Kagami, M. Inaba, and H. Inoue, "Motion planning for humanoid robots under obstacle and dynamic balance constraints," in *Proc. IEEE Int. Conf. Robot. Autom.*, 2001, pp. 692–698.

[15] N. E. Leonard, "Stability of a bottom-heavy underwater vehicle," *Automatica*, vol. 33, no. 3, pp. 331–346, 1997.

[16] P. Lotstedt, "Coulomb friction in two-dimensional rigid body systems," *Zeitschrift Angewandte Mathematik Mechanik*, vol. 61, pp. 605–615, 1981.

[17] A. Madhani and S. Dubowsky, "Motion planning of mobile multi-limb robotic systems subject to force and friction constraints," in *Proc. IEEE Int. Conf. Robot. Autom.*, 1992, pp. 233–239.

[18] D. W. Marhefka and D. E. Orin, "Gait planning for energy efficiency in walking machines," in *Proc. IEEE Int. Conf. Robot. Autom.*, 1997, pp. 474–480.

[19] M. T. Mason and Y. Wang, "On the inconsistency of rigid-body frictional planar mechanics," in *Proc. IEEE Int. Conf. Robot. Autom.*, 1988, pp. 524–528.

[20] R. Mason, J. W. Burdick, and E. Rimon, "Stable poses of 3-dimensional objects," in *Proc. IEEE Int. Conf. Robot. Autom.*, 1997, pp. 391–398.

[21] R. Mason, E. Rimon, and J. W. Burdick. (1996). The stable poses of objects supported by multiple contacts. Dept. of ME, California Inst. Technol., Pasadena, Tech. Rep. [Online]. Available: http://robotics.caltech.edu/papers.

[22] R. Mattikalli, D. Baraff, P. Khosla, and B. Repetto, "Gravitational stability of frictionless assemblies," *IEEE Trans. Robot. Autom.*, vol. 11, no. 3, pp. 374–388, Jun. 1995.

[23] R. Mattikalli, D. Baraff, P. Khosla, and B. Repetto, "Gravitational stability of frictionless assemblies," *Int. J. Robot. Res.*, vol. 11, no. 3, pp. 374–388, 1995.

[24] R. B. McGhee and A. A. Frank, "On the stability properties of quadruped creeping gaits," *Math. Biosci.*, vol. 3, pp. 331–351, 1968.

[25] K. Mirza and D. E. Orin, "General formulation for force distribution in power grasps," in *Proc. IEEE Int. Conf. Robot. Autom.*, 1994, pp. 880–887.

[26] A. Nagakubo and S. Hirose, "Walking and running of the quadruped wall-climbing robot," in *Proc. IEEE Int. Conf. Robot. Autom.*, 1994, pp. 1005–1012.

[27] W. Neubauer, "Spider-like robot that climbs vertically in ducts or pipes," in *Proc. Int. Conf. Intell. Robots Syst. (IROS)*, 1994, vol. 2, pp. 1178–1185.

[28] T. Omata, K. Tsukagoshi, and O. Mori, "Whole quadruped manipulation," in *Proc. IEEE Int. Conf. Robot. Autom.*, 2002, pp. 2028–2033.

[29] T. Omata and K. Nagata, "Rigid body analysis of the indeterminate grasp force in power grasps," *IEEE Trans. Robot. Autom.*, vol. 16, no. 1, pp. 46–54, Feb. 2000.

[30] Y. Or and E. Rimon, "Robust multiple contact postures in a two-dimensional gravitational field," in *Proc. IEEE Int. Conf. Robot. Autom*, 2004, pp. 4783–4788.

[31] J. S. Pang and J. C. Trinkle, "Stability characterizations of fixtured rigid bodies with coulomb friction," in *Proc. IEEE Int. Conf. Robot. Autom.*, 2000, pp. 361–368.

[32] J. S. Pang and J. C. Trinkle, "Stability characterizations of rigid body contact problems with coulomb friction," *Zeitschrift Angewandte Mathematik Mechanik*, vol. 80, no. 10, pp. 643–663, 2000.

[33] E. Rimon and J. W. Burdick, "A configuration space analysis of bodies in contact. Part I. 1st order mobility," *Mech. Mach. Theory*, vol. 30, no. 6, pp. 897–912, 1995.

[34] E. Rimon and J. W. Burdick, "A configuration space analysis of bodies in contact. Part II. 2nd order mobility," *Mech. Mach. Theory*, vol. 30, no. 6, pp. 913–928, 1995.

[35] E. Rimon and J. W. Burdick, "Mobility of bodies in contact. Part I. A 2nd order mobility index for multiple-finger grasps," *IEEE Trans. Robot. Autom.*, vol. 14, no. 5, pp. 696–708, Oct. 1998.

[36] E. Rimon and J. W. Burdick, "Mobility of bodies in contact. Part II. How forces are generated by curvature effects," *IEEE Trans. Robot. Autom.*, vol. 14, no. 5, pp. 709–717, Oct. 1998.

[37] E. Rimon, R. Mason, J. W. Burdick, and Y. Or. (2007). Application of a stratified-Morse-theory stance stability test to quasistatic locomotion planning. Dept. ME, California Inst. Technol., Pasadena, Tech. Rep. [Online]. Available: http://robotics.caltech.edu/papers.

[38] W. Thompson and P. G. Tait, *Treatise on Natural Philosophy*. Cambridge, U.K.: Cambridge Univ. Press, 1886.

[39] J. C. Trinkle, A. O. Farahat, and P. F. Stiller, "First-order stability cells of active multi-rigid-body systems," *IEEE Trans. Robot. Autom.*, vol. 11, no. 4, pp. 545–557, Aug. 1995.

[40] J. C. Trinkle, A. O. Farahat, and P. F. Stiller, "Second-order stability cells of a frictionless rigid body grasped by rigid fingers," in *Proc. IEEE Int. Conf. Robot. Autom.*, 1994, pp. 2815–2821.

[41] Y. Yokokohji, S. Nomoto, and T. Yoshikawa, "Static evaluation of humanoid robot postures constrained to the surrounding environment through their limbs," in *Proc. IEEE Int. Conf. Robot. Autom.*, 2002, pp. 1856–1863.

[42] T. Yoshikawa, "Passive and active closure by constraining mechanisms," *J. Dyn. Syst., Meas., Control*, vol. 121, no. 3/4, pp. 418–424, 1999.

E. Rimon (M'96), photograph and biography not available at the time of publication.

R. Mason (M'05), photograph and biography not available at the time of publication.

J. W. Burdick (M'05), photograph and biography not available at the time of publication.

Y. Or, photograph and biography not available at the time of publication.